UNIVERSITY OF CALIFORNIA, SAN DIEGO

Improved Global Bathymetry, Global Sea Floor Roughness, and Deep Ocean Mixing.

A dissertation submitted in partial satisfaction of the requirements for the degree

Doctor of Philosophy

in

Earth Sciences

by

Joseph Jeffrey Becker

Committee in charge:

David T. Sandwell, Chair
Steven C. Cande
Sarah T. Gille
Stefan Llewellyn Smith
Robert L. Parker

2008

The Dissertation of Joseph Jeffrey Becker is approved, and it is acceptable in quality and form for publication on microfilm:

_____

_____

_____

_____

_____

Chair

University of California, San Diego

2008

To Shari, Angela, and Mrs. Grunwald.

I have reached an age when, if someone tells me to wear socks, I don't have to.

Albert Einstein

Table of Contents

List of Figures

Acknowledgements

The truism is that one's committee should provide guidance and be helpful with the research. Often that is not the case, but in my own research everyone was in fact part of this work. In many ways I simply typed their thoughts into my trusty laptop.

Dave Sandwell provided the funding, training, and guidance that he lavishes upon all his students. His door is always open, and his advice always generous and helpful. Beyond those professional aspects, Dave stood by me during the most difficult period of my life; days so dark that nearly everyone else including my wife and family deserted me. He is a role model for me and all around him.

Bob Parker taught the best class of my graduate career and wrote up a brief 40 page note detailing the calculations I needed to estimate the power spectrum of topography using single beam sonar.

Steve Cande was the first faculty member I met when I arrived at SIO. In addition to helping me get rolling with the GMT software, he demonstrated a zest for adventure at sea that help lead me to enroll in the PhD program.

Sarah Gille pointed out several areas where my research needed additional work and provided the essential human factors guidance for my degree.

Stefan Llewellyn Smith is the unusual case of an "outside advisor" that actively researches in my field. His many fine articles provided the theory that I based my research plan upon.

Bruce Bills was the essential sounding board for all my crazy ideas, even the scientific ones. Bruce is an authority on planetary topography and tidal effects the key ideas of this work. I could not have done it with out your knowledge and help.

In addition to my committee I'd like to thank a few friends and colleagues. Jeff Dingler was serving in Iraq when I began squatting in his office. Fortunately we hit it

off, and we have had a wonderful 4 years of lively and far ranging conversations. Danny Brothers soon joined the circus and even managed to teach me the few things I know about rocks.

I'd like to thank Dick Norris for asking the off hand question, "What are you going to do with your PhD?" This is an excellent question, and four years later I remained stumped. Neal Driscoll graciously pointed out that nobody is going to give a 50 year with a recent PhD a tenure track position, so the problem is not completely open ended.

Every graduate student eventually learns a deadline is the real secret to graduating from graduate school. Lisa Tauxe graciously provided me a chance to teach SIO 1 and hence a deadline. This is also a dream come true: teaching physics at college.

The text and figures from chapter 3 are being prepared for publication in JGR Oceans as Becker, J. J. and Sandwell, Global Estimates of Sea floor Slope from Single-Beam Ship Soundings The dissertation author was the primary researcher and author of the submitted work. The coauthor directed and supervised that research, which forms the basis for this chapter.

Vita

1977	Bachelor of Art, Physics Harvey Mudd College
1978	Master of Science, Physics University of Chicago
1978-2001	Engineer HP, Apple, NeXT, Cisco, Broadcom
2001-2002	Retired
2008	Doctor of Philosophy, Earth Sciences Institute of Geophysics and Planetary Physics Scripps Institution of Oceanography University of California, San Diego

Publications

Becker, J. J., and Sandwell, D. T. (2008), Global Estimates of Sea floor Slope from Single-Beam Ship Soundings, In Press, J. Geophys. Res.

Abstract of the Dissertation

Improved Global Bathymetry, Global Sea Floor Roughness, and Deep Ocean Mixing.

by

Joseph Jeffrey Becker

Doctor of Philosophy in Earth Sciences

University of California, San Diego, 2008

David T. Sandwell, Chair

The resolution of existing satellite bathymetry was limited by the paucity and accuracy of the sounding used in its construction. A ongoing campaign to gather all unclassified soundings increased the number of sounding by an order of magnitude. Specialized software was written and used to edit more than 250 million soundings for accuracy. The result is a bathymetry gridded four times more finely than the current state of the art and is of general interest. The edited data was also used to make a global map of sea floor roughness that indicates significant amounts of deep ocean mixing may be occurring in unexpected locations; the Southern Ocean in particular.

1

Introduction

Maps are perhaps the most fundamental of the tools used in earth science. No one plans fieldwork with out consulting a map of the area. Once at the site, making a map is typically the first order of business. After the data is collected and analyzed, it is frequently presented as part of a new map that facilitates future research.

Radar and optical imaging allowed complete mapping of all the objects in the solar system except the ocean floor. Research vessels using multi-beam sonar make an occasional detailed map of the small parts of the ocean basins. Yet the bottom of the ocean continued to be a largely unmapped locality. That might have continue to have been true for the foreseeable future, but remarkable progress has been made using radars flying in outer space to measure the bottom of the ocean in a subtle and in many ways remarkable fashion.

Light penetrates only a few 100 meters into the ocean depths and cannot be used to directly visualize seafloor topography. Light, and radar, reflects away from its source off the surface of the ocean. This leads to the perhaps paradoxical observation that water appears black in a radar image as most of the energy is reflected away from the observer, whereas land areas scatter the incident energy in many directions. When a radar in space

is pointed exactly down, a very strong echo is returned. With enough careful engineering an extremely precise measurement of a satellite's altitude can be made. The exact location of the radar can be determined using GPS satellites and an extremely accurate map of the surface of the ocean created.

What possible use can a map of the surface of the ocean be? After all the surface of the ocean is "flat" outside of the random waves that ripple across it's surface. What's there to map? As it turns out the surface of the ocean has a topography that is many ways richer than that of land. Land topography does respond to tides and tectonic forces but the displacements are relatively subtle. The surface of the ocean has a very dynamic shape that changes moment by moment in response to winds, tides, currents, changes in temperature, and a host of other processes. In particular the topography of the ocean corresponds in a remarkable way to the topography of the ocean floor.

A fluid moves in a complex and fascinating ways, but the motion of interest here the response of a fluid to changes in gravity. Because water flows, a local disturbance such as a wave is pulled by gravity back to mean surface. Gravity changes (slightly) from location to location, and the ocean moves until it forms a surface of constant gravitational potential. By mapping the topography of the ocean surface, the geoid's shape is mapped. The source of gravity is mass, and the distribution of mass in the Earth determines the gravitational potential at any location inside or outside the Earth. Unfortunately the gravitational field of the Earth does not uniquely determine the distribution of the mass in the Earth.

This unfortunate result leads some to dismiss gravity measurements as uninteresting. However, the density contrast of water and rock at the ocean floor is so large, that the variation of the geoid at sea depends to first order on the depth of the ocean; at least over distances on the order of 10-200 km. The detailed calculations require accounting for the convolution of the bottom topography with the composition of the

rocks in the locality, but in essence, rock is more massive than water and hence gravity is stronger above a seamount than a deep trench. The geoid, (ocean surface), is thus slightly higher above a seamount and lower over a trench.

There are limitations on the accuracy of the method because of the confounding effects of winds, tides, and currents, but measurements of the geoid combined with the limited sonar bathymetry have provided increasingly accurate maps of global topography. Previous research by David T. Sandwell and others provide the gravity measurements that are the fundamental basis of this dissertation.

Although radar altimetry has been an efficient tool for mapping global ocean basins, the resolution of the method is 10 km at best. The main limitation is the smoothing effect on the gravity field variations due to observing gravity 3-5 km above the ocean floor.

Higher resolution can only be obtained by other methods, in particular sounding made by ships. Single beam echo sounders measure the depth of a small patch of the seafloor directly under the ship. These depth measurements can be very accurate, although many of them were taken long before GPS made navigation a trivial task. Under extreme conditions, navigation errors are common, but the "ancient" soundings collected 50 years ago are still valuable because they are often the only high latitude soundings available. In the past, satellite bathymetry was forced to exclude entire cruises because there was no way to remove even a small number of badly navigated soundings. A major topic of this research has been the development of tools and techniques that rescue the many good soundings that have been collected with bad navigation. In addition to bad navigation, there are many other sources of error [*Smith*, 1993], and few of them can be detected, let along corrected, automatically. The situation is further complicated by the wide range of ships and organizations represented in the historical archives. The approach taken was to create a software application that compares soundings to the smoother

gravity derived bathymetry.

Modern ships with modern sonar make multibeam soundings that cover a wide swath of the seafloor. Although there are multibeam sounding taken before the wide spread use of GPS, typically multibeam soundings are well navigated. Multibeam data still needs to be "processed" or edited to bring out its full quality because artifacts are usually present due to faulty temperature profiles, malfunctioning or fouled transducers, and a wide range of other problems. Rather than reprocess multibeam data, it was decided to treat multibeam data a collection of single beam and use the single beam tools to review and edit it. Unfortunately, this approach is sub-optimal because multibeam data is so voluminous that it slows the editing to a crawl, making a painstaking process a tedious and painstaking one.

However, the main problem with multibeam data is that only a tiny fraction of the ocean has been mapped with multibeam data and any bathymetry using all the sonar data available has to ingest data in some locations sampled with multibeam every 200m, and in other locations there could be hundreds of kilometers between single beam ship tracks.

The second chapter of this thesis describes a 3-year effort to gather and assimilate all sounding collected over the last 50 years by more than 5,000 cruises. The process involved the development of software applications and collection and editing of over 250 million soundings. The edited soundings were combined with the latest land and satellite bathymetry. The result is perhaps the best global bathymetry currently available.

This new bathymetry is titled "SRTM30_PLUS" and is remarkably better in some ways. In places with large amounts of sonar data, the grid spacing is 30 arc-seconds, four times better linear spacing, or 16 more samples per unit area than the widely used [*Smith and Sandwell*, 1997] bathymetry. Secondly, the sparse single beam data has been edited and many obvious errors are been removed.

More importantly, we can use this clean data to measure the roughness of the

seafloor globally. Walter Munk and others have proposed that the tides mix the ocean basins [*Munk*, 1966; *Munk and Wunsch*, 1998], with the implication that "seamounts are the stirring rods of the ocean". The problem is that there are not enough seamounts to do the job. Another source of mixing is the small but steep abyssal hills, (1 km wide by 100 m high), formed at the mid-ocean ridges. Abyssal hills are ubiquitous and could provide the missing mixing.

The third chapter is a paper published in JGR Oceans that uses the same data in a novel way to create a global map of the slope (roughness) of the seafloor. The detailed results allow climate researchers and physical oceanographers to improve their models of ocean mixing and hence climate change. The overall result is that most of the rough topography is not where most of the ocean mixing experiments are being done. This suggests that additional experiments are needed primarily in the Southern Ocean, and that models of climate change maybe in need of revision.

1.1 REFERENCES

Munk, W. (1966), Abyssal Recipes, *Deep-Sea Research Part I-Oceanographic Research Papers*, *13*, 707-730.

Munk, W., and C. Wunsch (1998), Abyssal recipes II: energetics of tidal and wind mixing, *Deep-Sea Research Part I-Oceanographic Research Papers*, *45*(12), 1977-2010.

Smith, W. H. F. (1993), On the Accuracy of Digital Bathymetric Data, *Journal of Geophysical Research-Solid Earth*, *98*(B6), 9591-9603.

Smith, W. H. F., and D. T. Sandwell (1997), Global sea floor topography from satellite altimetry and ship depth soundings, *Science*, *277*(5334), 1956-1962.

2

Global Bathymetry and Elevation Data at 30 Arc Seconds Resolution: SRTM30_PLUS

2.1 ABSTRACT

A new 30-arc second resolution global topography (SRTM30_PLUS) is available for download. The data combines dense SRTM30, ICESat, and GEBCO elevation data with 263 million edited soundings interpolated by a 1-minute bathymetry derived from satellite altimetry. The data format is the same as the 33 SRTM30 tiles, and the data's provenance is available.

2.2 INTRODUCTION

The depth to the ocean floor and the roughness of the bottom vary throughout the oceans because of numerous geologic processes [*Brown et al.*, 1998]. This seafloor topography (Figure 1) influences the ocean circulation and mixing that moderate Earth's climate [*Kunze and Llewellyn Smith*, 2004; *Munk and Wunsch*, 1998], and the biological diversity and food resources of the sea [*Koslow*, 1997]. The ocean floor records the geologic history and activity of the ocean basins [*Muller et al.*, 1997], revealing areas that may store resources such as oil and gas [*Fairhead et al.*, 2001], and generate earthquakes and tsunamis [*Mofjeld et al.*, 2004]. Despite the importance of Earth's ocean floor to our quality of life, we have made much better maps of the surfaces of other planets, moons, and asteroids.

After five decades of surveying by ships carrying echo sounders, most of the ocean floor remains unexplored and there are large gaps between survey lines (Figure 2a). There are two primary reasons why the global mapping of the seafloor is so incomplete. First, seafloor mapping is difficult, expensive, and slow. For example, a systematic mapping of the deep oceans by ships would take more than 120 years of survey time. Moreover, because the swath width of a multibeam echo sounder is proportional to depth, it takes much longer (750 ship-years) to survey the shallow (< 500 m) continental margins [*Carron et al.*, 2001]. The second reason is that the existing raw sounding data sets are extremely heterogeneous. Most of the data in remote ocean basins were collected during an era of curiosity-driven exploration (1950 – 67), depths were measured by single-beam analog echo sounders, and satellite navigation was unavailable [*NGDC*; *Smith*, 1993]. Recent deep ocean surveys using advanced technology (i.e., GPS navigation and multi-beam acoustic swath mapping systems) are funded through a peer-review system emphasizing hypothesis testing; the result is that ships tend to re-visit a

limited number of localities. Thus the majority of the data in the remote ocean basins are old and of poor quality. These remarks apply to publicly available data; additional data exist that are proprietarily held for commercial or political reasons, or are classified as secret for military purposes [*Smith*, 1998]. The largest such data set, the Ocean Survey Program of the U.S. Navy, covers primarily the northern oceans [*Medea*, 1995].

While shipboard surveys offer the only means for high-resolution seafloor mapping, moderate accuracy (~100 m) and resolution (12-17 km full wavelength) can be achieved using satellite radar altimetry at a fraction of the time and cost. Radar altimeters aboard the ERS-1 and Geosat spacecraft have surveyed the marine gravity field over nearly all of the world's oceans to a high accuracy and moderate spatial resolution of 25-45 km; [*Cazenave et al.*, 1996; *Sandwell and Smith*, 1997; *Tapley and Kim*, 2001]. In the wavelength band 10 to 160 km, variations in gravity anomaly are highly correlated with seafloor topography and thus, in principle, can be used to recover topography [*Baudry and Calmant*, 1991; *Dixon et al.*, 1983; *Jung and Vogt*, 1992; *Ramillien and Cazenave*, 1997; *Smith and Sandwell*, 1994]. The sparse ship soundings constrain the long wavelength (> 160 km) variations in seafloor depth and to calibrate local variations in the topography to gravity ratio associated with varying tectonics and sedimentation.

This study is focused on the production of a global bathymetry grid at 30 arc seconds of resolution by combining the most up-to-date satellite bathymetry at 1 minute resolution [*Smith and Sandwell*, 2008] with a vastly larger and improved data base of ship soundings (Figure 2b). The main contributions summarized in this report are: assembly of an array of publicly available depth soundings from a wide variety of sources; statistical and visual assessment of all soundings through a comparison with a previously published 2-minute global bathymetry grid; hand editing of all suspect data (single beam trackline, multibeam swaths, sparse sounding, and contributed grids); and finally using these soundings to modify global satellite bathymetry based on the latest altimeter-derived

gravity models. The [*IBCAO*, 2001] arctic bathymetry is used north of 80 degrees. In addition, the global bathymetry grid is merged with global elevations based on a combination of SRTM30 topography [*Farr et al.*, 2007] (latitude < 55 deg), GTOPO30 topography [*USGS*, 1997] in the Arctic, and ICESat derived topography [*DiMarzio et al.*, 2007] in Antarctica. Previous versions of our global grid, (i.e. V8.2 [*Sandwell and Smith*, 2001; *Smith and Sandwell*, 1997]), contained a flag indicating whether a 2-minute cell was constrained by a depth sounding or whether it was interpolated from satellite gravity. This new global grid of depth has a companion grid that also contains a source identification number (SID) that is used to identify the data source for a particular 30-second grid cell. This companion grid is a source map used to identify problematic data.

2.3 DATA SOURCES

More than 250 million soundings are used to create SRTM30_PLUS topography (Figure 2a) and are from a very diverse range of sources. In many cases, the data is publicly available and can be downloaded. The CCOM UNH "Law of the Sea" multibeam grids [*CCOM*, 2008] include, Alaska and the Arctic, the Marianas, Kingman Reef and Palmyra Atoll, the Western Atlantic Ocean and the Gulf of Mexico. The RidgeMBS [*Marine Geoscience Data System*, 2008] data include multibeam grids from many mid-ocean ridges around the world. The JAMSTEC grids [*JAMSTEC*, 2008] are multibeam data primarily of the Japanese shelf and Western Pacific. IBCAO [*IBCAO*, 2001] Artic grids are used at high latitudes where satellite altimetry is less accurate. The bathymetry presented here is also constrained by the standard GEBCO contours [*GEBCO*, 2008].

The bulk of 5,000 ship tracks originally from NGDC has been edited at SIO and is stored there. Additional SIO cruises [*Miller*, 2008] that are not in the NGDC have

also been edited and used in this bathymetry. These cruises span more than 50 years of expeditions by many investigators on many ships. The *SIOExplorer* [*Miller*, 2008] is a long-term project to archive the data collected, gather as much meta data as possible, and provides a sophisticated web based user interface.

The 14 million soundings provided by IFREMER, NOAA, NAVO, and NGA is the sum of all their unclassified data and are from too many data sources to cite here. The interested reader should enquire directly to those agencies.

Many shallow water soundings have been contributed to this project by various volunteering hydrographic offices around the world, through this project's cooperation with GEBCO. International Hydrographic Organization Circular Letter 2007/14 requested HO's to harvest soundings from their Electronic Navigation Charts and send these to the International Hydrographic Bureau, for inclusion into future GEBCO releases. Mr. Tony Pharaoh of IHB and Ms. Pauline Weatherall of BODC have kindly supplied these data.

2.4 EDITING METHODS

Time series tools such as auto regressive (AR) filters and robust curve fitting do an excellent job of finding outliers points. Unfortunately, there is a large number of very diverse ways that data can be corrupted [*Smith*, 1993], and automated editing is less successful at discriminating and correcting these. To efficiently edit ~250 million soundings a software application, *cmEdit,* was written at SIO. Unlike existing, and more sophisticated, geophysical visualization programs, this simple tool is focused on one task: finding data blunders in MGD77 ship track data. Approximately 20 years ago Paul Wessel and Walter HF Smith, the developers of the Generic Mapping Tools (GMT) [*Wessel and Smith*, 1995], wrote a similar application called GMTEdit that was the inspiration for

this effort, but is completely unrelated. *cmEdit* is written in Objective-C using the Apple Xcode 3.0 development system, and runs on OSX 10.5.

The premise of our data editing is that "predicted" bathymetry is a low pass filtered representation of the actual topography. The "predicted" depth is the "unpolished" bathymetry measured with satellite altimetry. Visual comparison of ship data and the smooth predicted bathymetry frequently, but not always, illuminates a wide range of data blunders. Our goal was to allow an analyst to efficiently scan many millions of soundings for blatant, but difficult to parameterize data errors, and edit the errors. The intention is to rescue as much data as possible from the thousands of "known bad" ship tracks that have an occasional and obvious bad patch, but also have a substantial amount of useful data.

The files consist primarily of single beam sonar, although processed (gridded) multibeam data, and a small number of other data types are present. Because the editing task is only going to be done once, all the data is first converted to a 10-column text format so that the analyst and software developers can easily debug the various scripts and programs needed to convert the diverse data into a common format. Text files are also easy to use in ad hoc quality control studies. If the data were going into an application used daily and interactively, a binary representation of the data stored in a relational database would be more efficient. Currently the approximately 300 million data points stored as text data consumes about one hundred gigabytes of disk space; relatively small compared to some geophysical data sets, and perfectly manageable on a modern desktop computer.

The text file format contains 10 fields (Figure 4). The "time" field is simply a unique index given to every sounding (row) in that file. Typically, it is the distance logged from the last port, but the distance may be missing, so a Julian date or even a row number can be substituted. Each file can use a different index, but it does need to be monotonically increasing. The analyst's job is simplified if the actual time data is

available because it makes a data gap immediately apparent.

The latitude, longitude, and depth fields must be populated and in units of degrees (+/-180) and meters (sea level 0, depths negative). The horizontal and depth uncertainties (meters) could be used in the editing to provide error bars, but are currently reserved and unused. The "predicted" depth is the "unpolished" bathymetry measured with satellite altimetry. Because the gravity data used to generate the predicted bathymetry does not contain wavelengths shorter than about 20 km, it provides a smoothly varying nominal depth to compare against the actual soundings. After the sounding data is edited they are combined with predicted bathymetry to smoothly go through each sounding at a resolution of 30 arc seconds. The *cmEdit* program will accept a zero source id, but data without a source id was not acceptable for quality control reasons.

2.5 GRIDDING METHOD

A new feature of the data presented here is that it maintains the source identification number (SID) of each sounding used to make the polished bathymetry. Quality control is greatly improved because the provenance of each sounding is known. In addition to the GMT utilities [*Wessel and Smith*, 1995], a specialized form of *blockmedian* that calculates the median value of the data and the SID of that median value was written. The code for *medianId* is virtually identical to *blockmedian*, supports all the existing features and flags, and consists of only a dozen additional lines of C code. The rest of the processing is essentially an exercise in using *awk* and various GMT utilities to produce a bathymetry grid and a source grid with the SID of each sounding.

The processing details are to gather 263 million edited soundings from 9,974 unique sources and sort them with *awk* into the 33 SRTM tiles. To avoid edge effects during filtering and computational nuisances at longitude 180 degrees, each tile is

extended 1 degree in each direction to create a boundary that is trimmed off after interpolation. The result is 33 large files, each with millions of essentially randomly located soundings. Each is processed with *medianId* to combine soundings that are closer than the SRTM30_PLUS grid spacing into a single value. However, there is no data for the vast majority of the grid because so little of the ocean floor has been mapped. This is where the predicted data is used in an interpolation described as "polishing" in [*Smith and Sandwell*, 1997]. The value of the predicted bathymetry at each sounding is subtracted from the sounding, the difference is interpolated with *surface*, and then value of the predicted bathymetry is added back to the interpolated difference. The result is a "polished" grid that passes smoothly through each sounding, and has the value of the predicted bathymetry far from any sounding.

2.6 RESULTS

The bathymetry presented here (Figure 1), and available for download via FTP [*Becker*, 2008] improves the [*Smith and Sandwell*, 1997] global bathymetry in four ways. First, the number of soundings used here is an order of magnitude greater, and the soundings previously used in [*Smith and Sandwell*, 1997] have received additional editing. Second, the gravity model from [*Sandwell and Smith*, 2008] used in [*Smith and Sandwell*, 2008] to generate the predicted bathymetry has grid spacing twice as fine as [*Sandwell and Smith*, 1997], with half the noise, and extends to latitudes as high as 81 degrees. Third, the use of SRTM30 [*Farr et al.*, 2007] and GLAS [*DiMarzio et al.*, 2007], improves the land data. Finally, the use of [*IBCAO*, 2001] in the arctic improves that bathymetry. As discussed next, the overall improvement is considerable (Figure 1).

One general improvement clearly visible is the greatly reduced number of ship track artifacts. The [*Smith and Sandwell*, 1997] global bathymetry in the area around the Hawaiian Islands (Figure 5a) had a number of artifacts caused by ship tracks with

errors that have been edited from this bathymetry (Figure 5b). The fracture zones and ridges running roughly southwest to northeast are now clearly distinct from the artifacts present in the [*Smith and Sandwell*, 1997] global bathymetry. In addition to the reduction of artifacts, the improved gravity model [*Sandwell and Smith*, 2008] used in [*Smith and Sandwell*, 2008] predicted bathymetry reduced the noise on the seafloor and improved the overall resolution.

A general problem for altimetrically estimated depth is presence of deep sediments near continental margins. As discussed in [*Smith and Sandwell*, 1994], increasing sediment thickness decreases the correlation between gravity and depth and decreases the number of meters of depth variation that should be estimated from every milliGal of gravity variation. The [*Smith and Sandwell*, 1994] recipe deals with this in the "Inverse Nettleton procedure" where heavily sedimented areas are detected and the pre-polishing result is a flat seafloor. However there have to be enough soundings for the procedure give a good answer, and where there are fewer, it may create a falsely "dimpled" surface. An example of this artifact can be seen in the [*Smith and Sandwell*, 1997] global bathymetry of the Northeast Arabian Sea (Figure 6a). Our new bathymetry has a large number of soundings on the continental margin (Figure 2b) that constrain the predicted bathymetry enough to remove most of the sediment artifacts (Figure 6b).

The 263 million edited soundings used cover a substantial portion of the world's oceans (Figure 2a. However, many of these soundings are from multibeam data (~200m grid) that are averaged together at 30 arc seconds. Counting only nodes constrained by data other than the interpolated Artic grid, [*IBCAO*, 2001], the SRTM30_PLUS data has 39 million constrained nodes. Thus SRTM30_PLUS has more than six times as many constrained nodes as the [*Smith and Sandwell*, 1997] global bathymetry. This is partly due to an increase in the sounding data and partly due to the four fold reduction in the cell size from 2-minutes to 30-seconds.

To further quantify this large increase in constrained nodes, a simple calculation was done to remove the effects of the higher latitudes covered and smaller SRTM30_ PLUS grid spacing. The SRTM30_PLUS grid was down sampled by 4x (16x in area) to 2 minutes, limited to +/-72 degrees of latitude, and compared to the 2-minute [*Smith and Sandwell*, 1997] global bathymetry. The new constraints (Figure 2b) near shore are prominent and are one of our most important results. Even averaged down to 2-minute resolution, SRTM30_PLUS has approximately 50% more constraints than the [*Smith and Sandwell*, 1997] global bathymetry. The total coverage of control data is now 85 million sq. km, about 24% of the ocean floor

2.7 ERRORS ANALYSIS

A detailed assessment of each sounding's accuracy is currently in process. When the assessment is completed, the *blockmean, blockmedian,* or *medianId* utility can use the assigned standard deviation to calculate a weighted mean. However, a source grid would no longer be possible as any node could have a value derived from many sources rather than the unique median value. Another approach would be to calculate two bathymetries, one the weighted mean and the other the median value with provenance. The improved accuracy of a weighted mean could be more important than retaining the provenance of the data. The [*Smith and Sandwell*, 1997] global bathymetry provides no provenance, but is widely used, suggesting that most users do not need the data source.

2.8 CONCLUSION

The SRTM30_PLUS global topography is a substantial improvement on the widely used [*Smith and Sandwell*, 1997] global bathymetry. SRTM30_PLUS was created with an order of magnitude increase in the number of soundings. Maintaining the

provenance of each sounding made it possible to identify and remove artifacts ranging from a single bad ping to entire ship tracks. The large number of soundings on the world's continental margins increases accuracy in deeply sedimented areas.

2.9 APPENDIX - ACCESSING BINARY SRTM30_PLUS DATA FILES

GMT users read binary SRTM30_PLUS files with the GMT tutility *xyz2grd* [*Wessel*, 2007].

```
set file = e020n40.Bathymetry.srtm
set region = '-R/20/60/-10/40'
xyz2grd $file $region -ZTLh -F –L -I30c –G$file.grd
```

The following fragment of MATLAB [*MathWorks*, 2007] reads a SRTM30_PLUS binary file and, just as an example, sets the land to zero.

```
topography = readImg(e020n40.Bathymetry.srtm, 4800)
bathymetry = topography;
bathymetry (find(topography>0)) = 0;

function topography = readImg(fileName, numCols)
% Read 16 bit SRTM30+ file, and keep it int16 to save memory.

fid = fopen(fileName,'r');
[topography, cnt] = fread(fid, inf, 'int16=>int16');
fclose(fid);
```

```
% make image a rectangle. SRTM30+ has 4800 columns north of 60S,
% but 7200 columns south of 60S. So user has say how many…

numRows = cnt / numCols;
topography = reshape(topography, numCols, numRows)';

% On a "big endian" CPU, (e.g. Intel Mac), swap bytes.

topography = swapbytes(topography);
end
```

2.10 ACKNOWLEDGEMENTS

Scott Nelson, Seung-Hee Kim, and Breanna Binder cheerfully and accurately edited several hundred million single and multibeam soundings.

2.11 REFERENCES

Baudry, N., and S. Calmant (1991), 3-D Modeling of Seamount Topography from Satellite Altimetry, *Geophysical Research Letters*, *18*(6), 1143-1146.

Becker, J. (4 JAN 2008). Satellite Geodesy, IGPP, SIO, UCSD | Global Topography | SRTM30, Multibeam, & Predicted. http://topex.ucsd.edu/WWW_html/srtm30_plus.html (14 FEB 2008).

Brown, J., et al. (1998), *The Ocean Basins: Their Structure and Evolution*, 171 pp., Pergamon Press, Oxford.

Carron, M. J., et al. (2001), A proposed international long-term project to systematically map the world's ocean floors from beach to trench: GOMaP (Global Ocean Mapping Program), *Inter. Hydr. Rev.*, *2*(3), 49-50.

Cazenave, A., et al. (1996), High-resolution mean sea surface computed with altimeter data of ERS-1 (geodetic mission) and Topex-Poseidon, *Geophys J Int*, *125*(3), 696-704.

CCOM (11 FEB 2008). Law of the Sea : Center for Coastal and Ocean Mapping/Joint

Hydrographic Center - CCOM/JHC : Law of the Sea Data, UNCLOS, Article 76, extended continental shelf, foot of the slope, multibeam bathymetry, seafloor mapping, University of New Hampshire, UNH. http://ccom.unh.edu/index.php?p=39|46&page=law_of_the_sea.php (14 FEB 2008).

DiMarzio, J. P., et al. (5 Jan. 2007). GLAS/ICESat 500 m Laser Altimetry Digital Elevation Model of Antarctica. http://nsidc.org/data/nsidc-0304.html (5 Jan. 2007).

Dixon, T. H., et al. (1983), Bathymetric prediction from Seasat altimeter data, *J. Geophys. Res.*, *88*, 1563-1571.

Fairhead, J. D., et al. (2001), Satellite-derived gravity having an impact on marine exploration, in *The Leading Edge*, edited, pp. 873-876.

Farr, T. G., et al. (2007), The shuttle radar topography mission, *Reviews of Geophysics*, *45*(2), -.

GEBCO (12 DEV 2007). General Bathymetric Chart of the Oceans (GEBCO) Hom. http://www.ngdc.noaa.gov/mgg/gebco/ (14 FEB 2008).

IBCAO (24 Dec. 2003). IOC IHO IASC -International Bathymetric Chart of the Arctic Ocean (IBCAO). http://www.ngdc.noaa.gov/mgg/bathymetry/arctic/arctic.html (24 Dec. 2003).

JAMSTEC (n.d.). Deep Sea Research Data Web. http://www.jamstec.go.jp/dsr/index_eng.html (14 FEB 2008).

Jung, W. Y., and P. R. Vogt (1992), Predicting bathymetry from Geosat-ERM and shipborne profiles in the South Atlantic ocean, *Tectonophysics*, *210*, 235-253.

Koslow, J. A. (1997), Seamounts and the ecology of deep-sea fisheries, *Am Sci*, *85*(2), 168-176.

Kunze, E., and S. G. Llewellyn Smith (2004), The Role of Small-Scale Topography in Turbulent Mixing of the Global Ocean, *OCEANOGRAPHY*, *17*(1), 55.
Marine Geoscience Data System (n.d.). DMS:Ridge Bathymetry. http://www.marine-geo.org/rmbs/ (14 FEB 2008).

MathWorks, T. (2007), MATLAB, edited, The MathWorks, Natick, MA.

Medea (1995), *Scientific Utility of Naval Environmental Data*, 52 pp., MEDEA Office, McClean Virginia.

Miller, S. P. (n.d.). SIOExplorer. http://nsdl.sdsc.edu/ (14 FEB 2008).

Mofjeld, H. O., et al. (2004), Tsunami scattering and earthquake faults in the deep Pacific Ocean, *Oceanography*, *17*(1), 38-46.

Muller, R. D., et al. (1997), Digital isochrons of the world's ocean floor, *Journal of Geophysical Research-Solid Earth*, *102*(B2), 3211-3214.

Munk, W., and C. Wunsch (1998), Abyssal recipes II: energetics of tidal and wind mixing, *Deep-Sea Research Part I-Oceanographic Research Papers*, *45*(12), 1977-2010.

NGDC (11 Jan. 2006). GEODAS Search Criteria Selection. http://ftp.ngdc.noaa.gov/mgg/gdas/gd_cri.Html (2 Jan. 2008).

Ramillien, G., and A. Cazenave (1997), Global bathymetry derived from altimeter data of the ERS-1 Geodetic Mission, *J Geodyn*, *23*(2), 129-149.

Sandwell, D., and W. H. F. Smith (2001), Bathymetric estimation, in *Satellite Altimetry and Earth Sciences: A Handbook of Techniques and Applications*, edited by L.-L. Fu and A. Cazenave, pp. 441-457, Academic Press, San Diego.

Sandwell, D. T., and W. H. F. Smith (1997), Marine gravity anomaly from Geosat and ERS 1 satellite altimetry, *Journal of Geophysical Research-Solid Earth*, *102*(B5), 10039-10054.

Sandwell, D. T., and W. H. F. Smith (2008), Global marine gravity from retracked Geosat and ERS-1 altimetry: Ridge segmentation versus spreading rate, *Manuscript in preperation*.

Smith, W. H. F. (1993), On the Accuracy of Digital Bathymetric Data, *Journal of Geophysical Research-Solid Earth*, *98*(B6), 9591-9603.

Smith, W. H. F., and D. T. Sandwell (1994), Bathymetric Prediction from Dense Satellite Altimetry and Sparse Shipboard Bathymetry, *Journal of Geophysical Research-Solid Earth*, *99*(B11), 21803-21824.

Smith, W. H. F., and D. T. Sandwell (1997), Global sea floor topography from satellite altimetry and ship depth soundings, *Science*, *277*(5334), 1956-1962.

Smith, W. H. F. (1998), Seafloor Tectonic Fabric From Satellite Altimetry, *Annual Review of Earth and Planetary Sciences*, *26*(1), 697-747.

Smith, W. H. F., and D. T. Sandwell (2008), *Manuscript in preperation*.

Tapley, B. D., and M. C. Kim (2001), Applications to Geodesy, in *Satellite Altimetry and Earth Sciences*, edited by b. L.-L. F. a. A. Cazenave, pp. 371-403, Academic Press, New York.

USGS (21 Jan. 1997). USGS (U.S. Geological Survey) EROS, Sioux Falls, SD http://edc.usgs.gov/products/elevation/gtopo30/gtopo30.html (31 Jan. 2008).

Wessel, P., and W. H. F. Smith (1995), New Version of the Generic Mapping Tools Released, *EOS*.

Wessel, P. (2 OCT 2007). http://gmt.soest.hawaii.edu/ (14 FEB 2008).

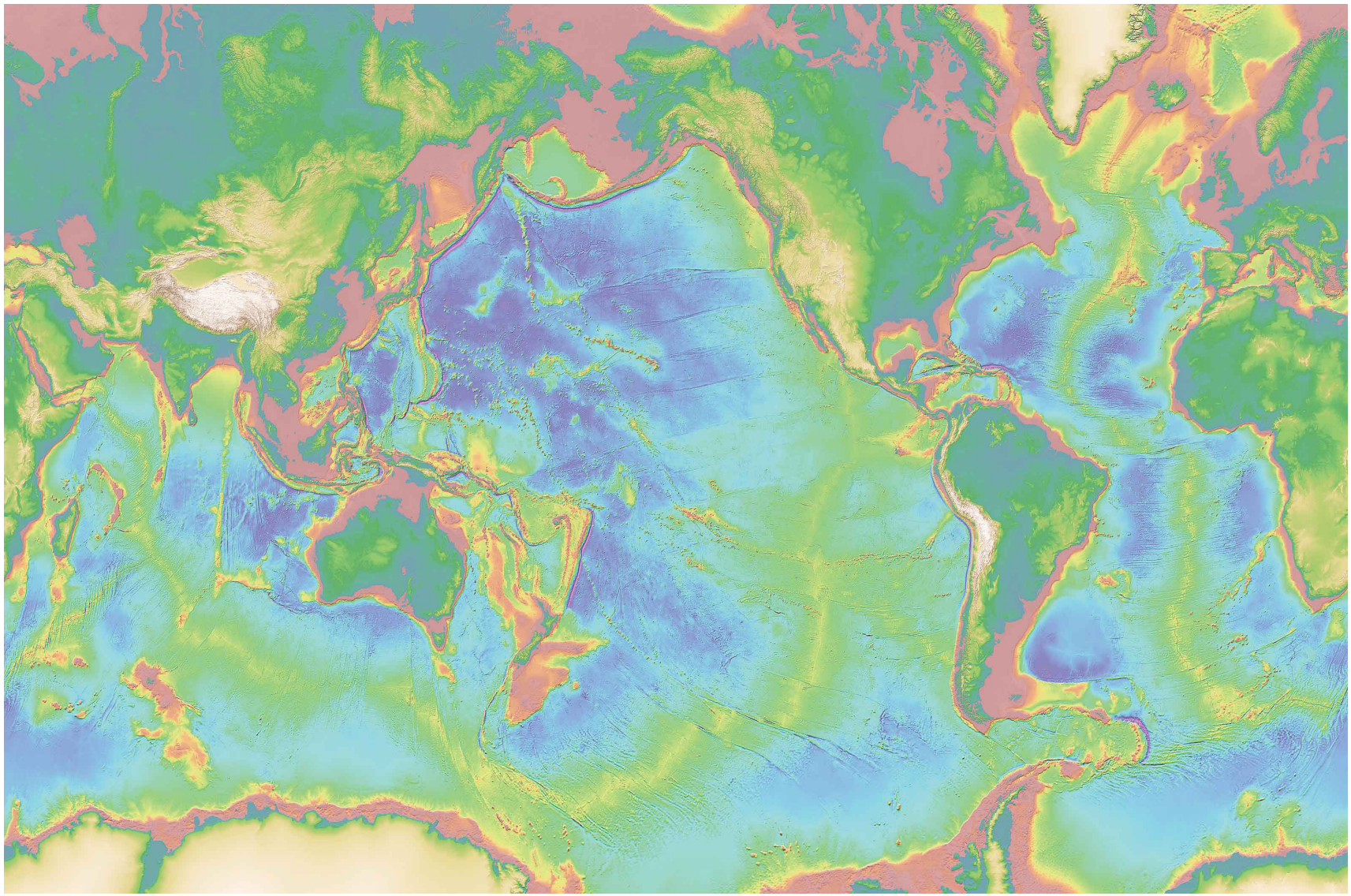

Figure 2-1: Bathymetry presented in this paper. The edited data has removed many obvious sea floor artifacts and the SRTM30 data improves the land.

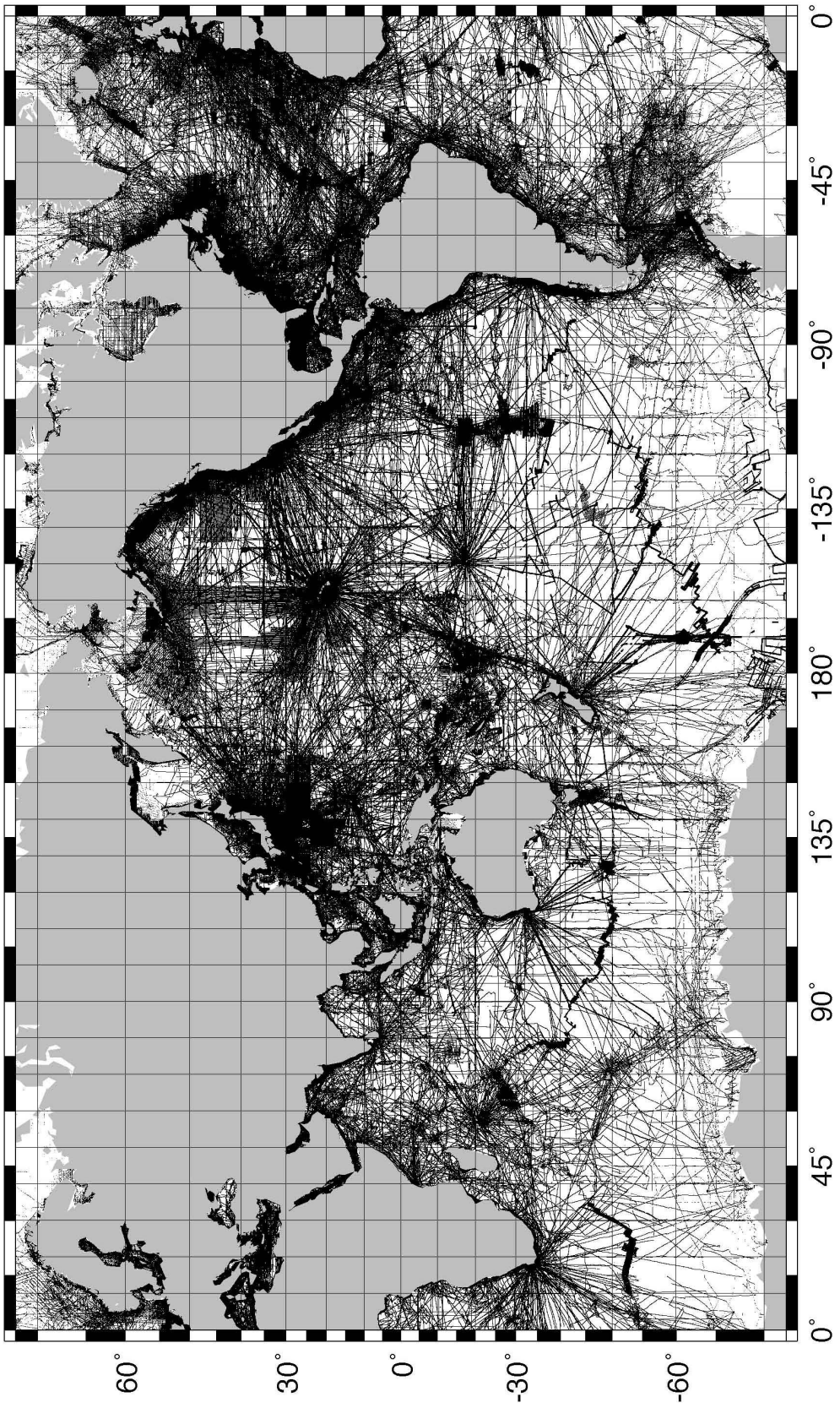

Figure 2-2: Ship track plot of soundings used in this paper.

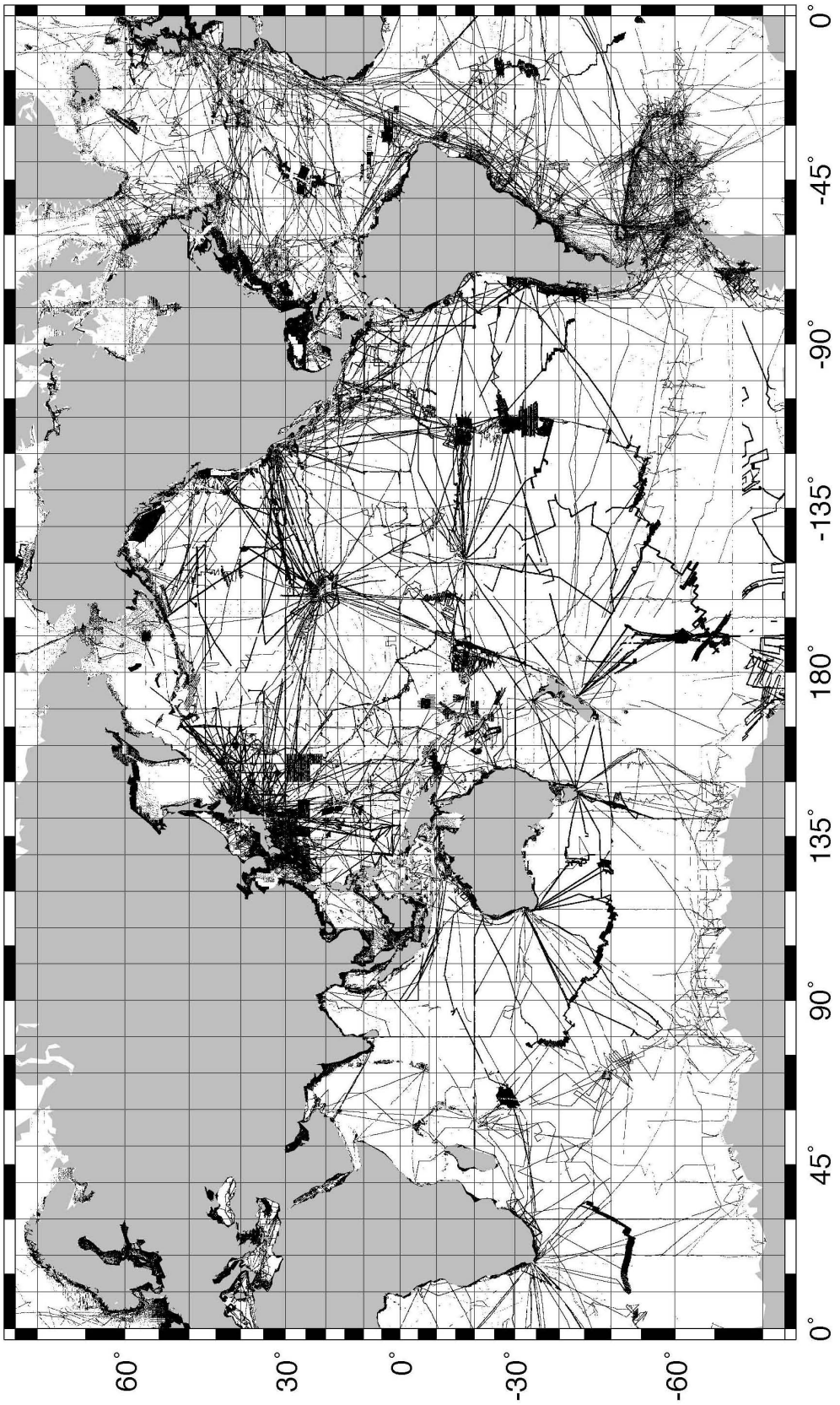

Figure 2-3: Ship track plot of soundings used in [*Smith and Sandwell*, 1997] global bathymetry

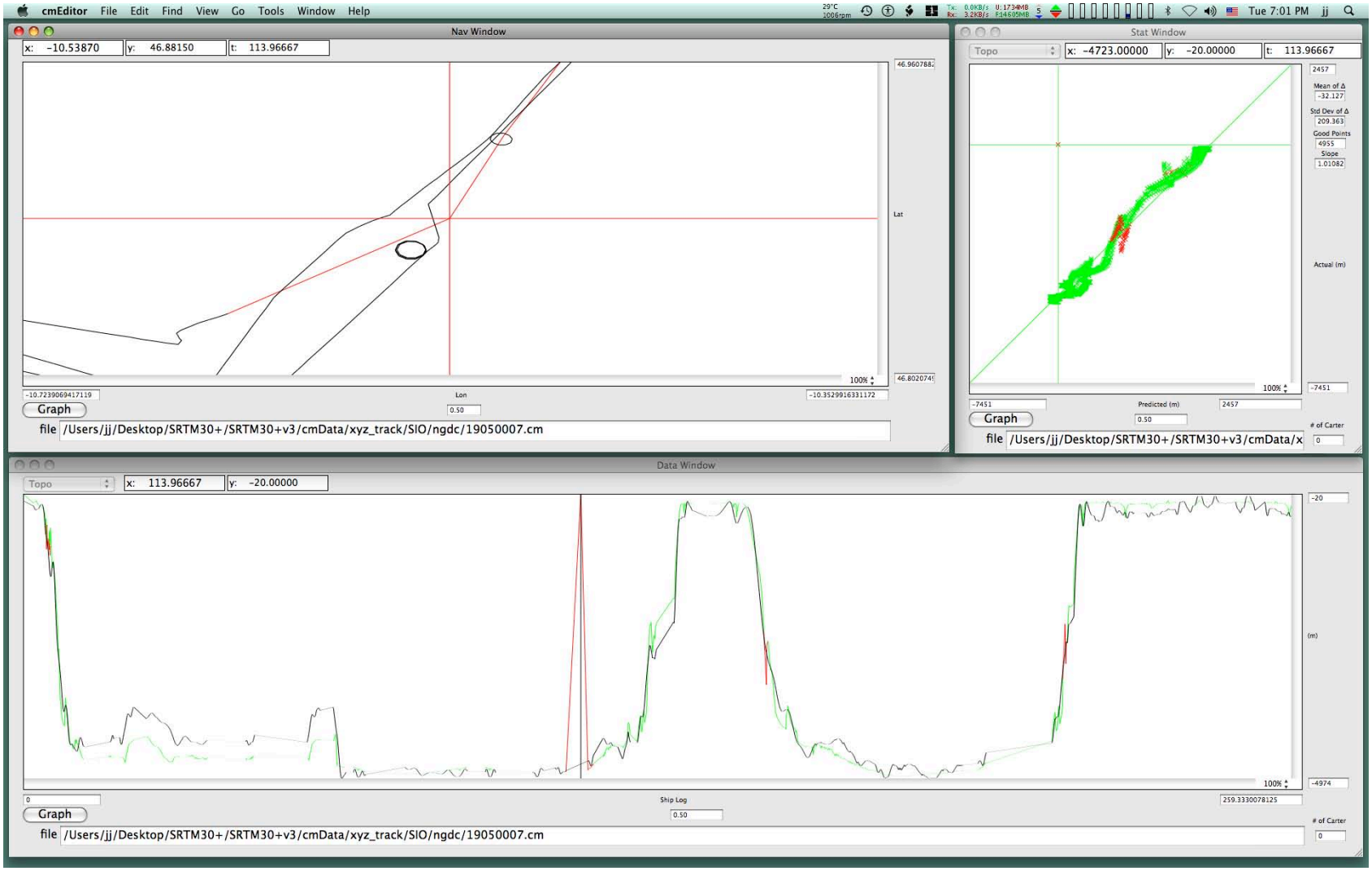

Figure 2-4: Screen shot of CM Edit showing the Navigation and Scatter windows on the left and the Data Window on the right. An outlier is selected in the Scatter window. The location of the outlier is displayed in the other windows as a graticle.

NAVO-NGA-NOAA-SIO DATA EXCHANGE FORMAT

The file is ASCII text and the precision of the data is variable and depends on the precision of the original data. There is white space between numbers.

time	time since an epoch (sec), or record sequence number
longitude	decimal degrees (+/- 180.)
latitude	decimal degrees (+/- 90.)
depth	depth; below sea level is negative (corrected meters)
sigma_h	estimated uncertainty in navigation (m) (0=no estimate)
sigma_d	depth uncertainty (m) (9999=edited data; -1= no estimate)
source_id	unique ID number for each source (0-65535). (NAVO uses 0 to 16383 NGA uses 16384 to 32767 NOAA uses 32768 to 49151 SIO uses 49152 to 65535)
pred_depth	predicted depth estimate (m) (used internally at SIO for editing)

An example from a multibeam grid from SIO cruise AVON07MV where the depth uncertainty is estimated to be 1 meter, but the navigation uncertainty is unknown:

TIME	LONGITUDE	LATITUDE	DEPTH	σ_H	σ_D	SID	PREDICTED DEPTH
1	-159.00500	31.08760	-5998	0	1	53914	-5780
2	-159.00200	31.06510	-5984	0	1	53914	-5796
3	-158.97100	31.06280	-5955	0	1	53914	-5805

Figure 2-5: “CM” data format that is used in the SIO dataset. SIO will accept processed bathymetry data in this format.

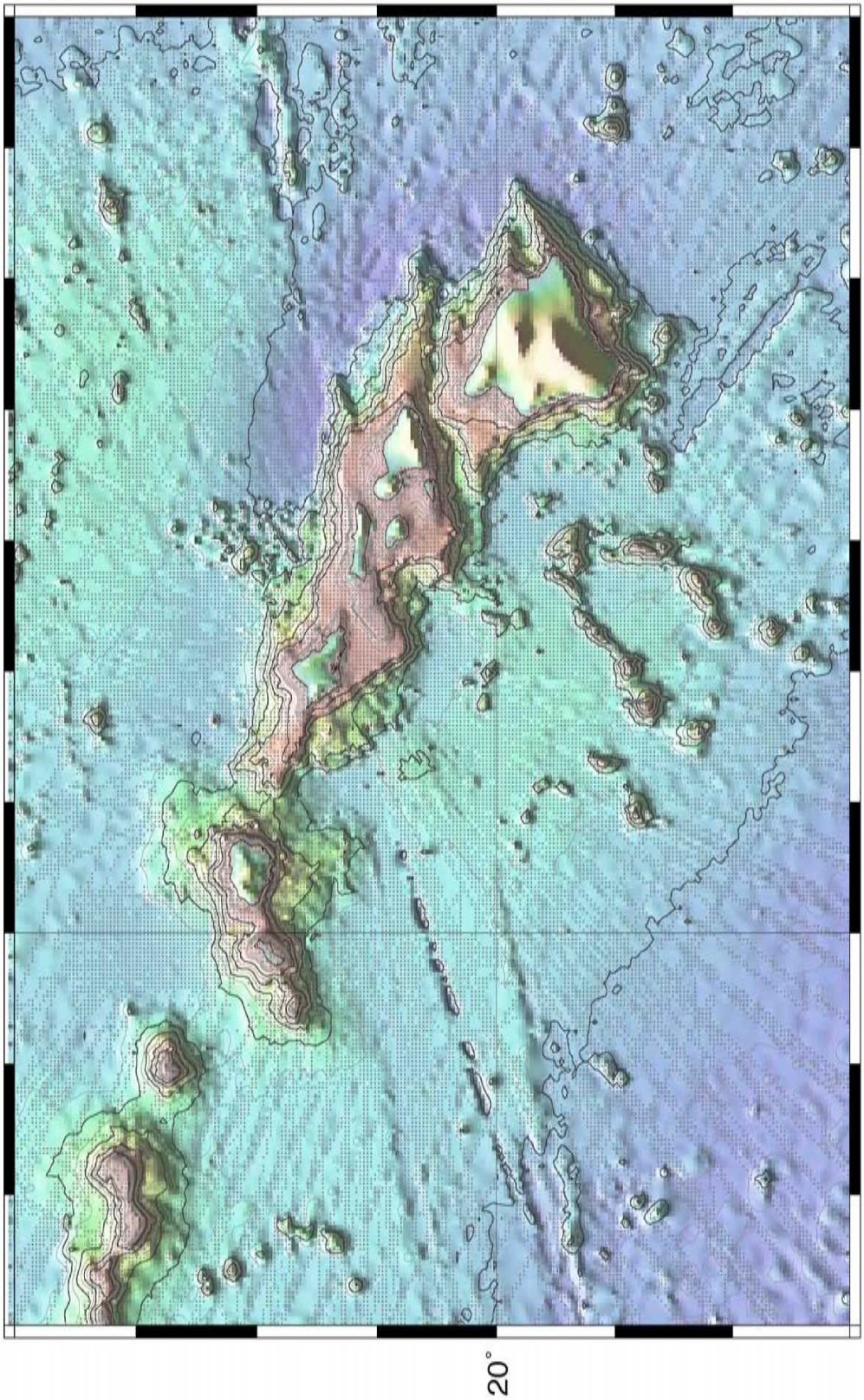

Figure 2-6: Hawaiian Islands from the [Smith and Sandwell, 1997] global bathymetry. Grey dots are soundings.

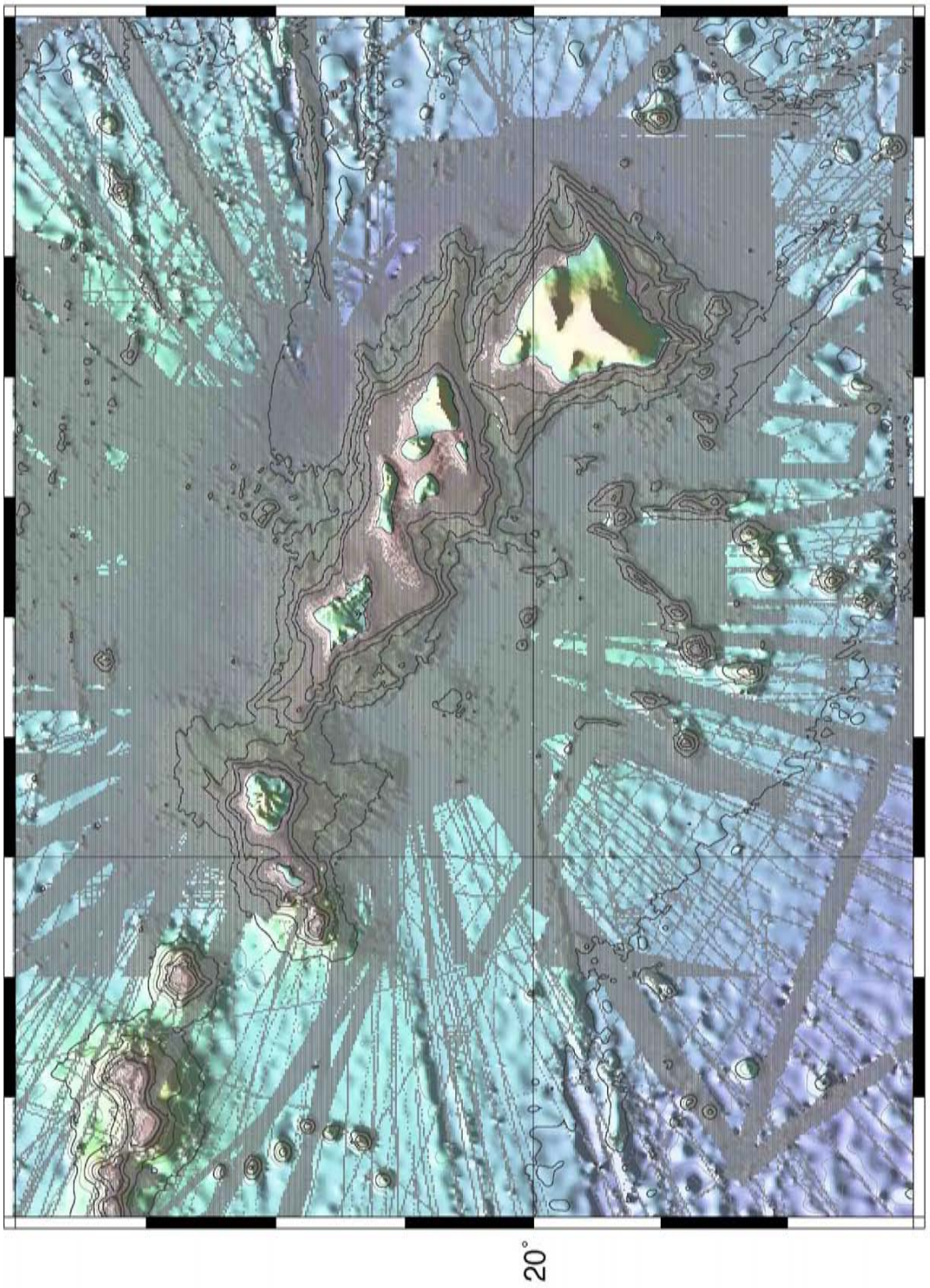

Figure 2-7: Hawaiian Islands from global bathymetry presented in this paper. Grey dots are soundings.

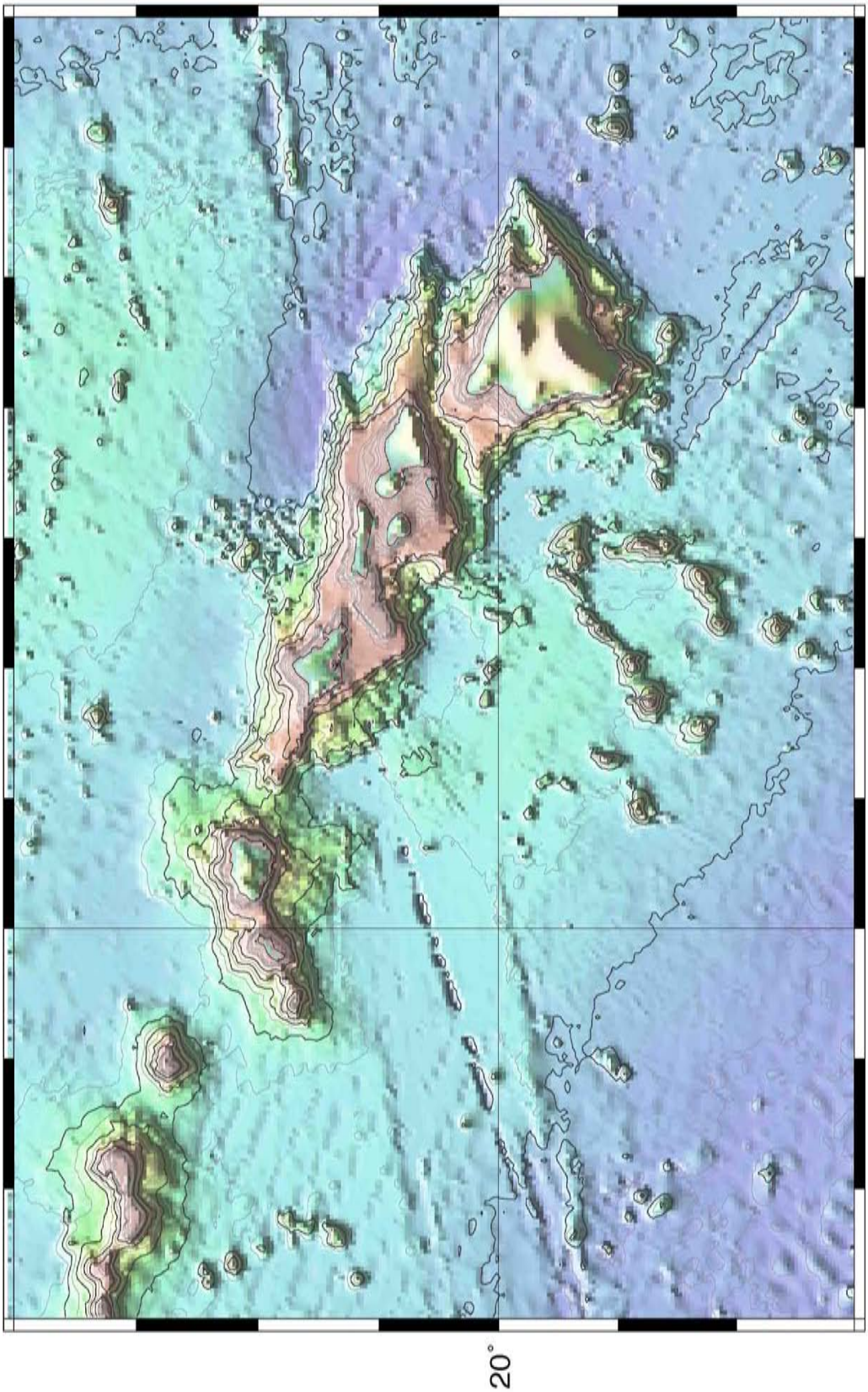

Figure 2-8: Figure 2-6, but without soundings.

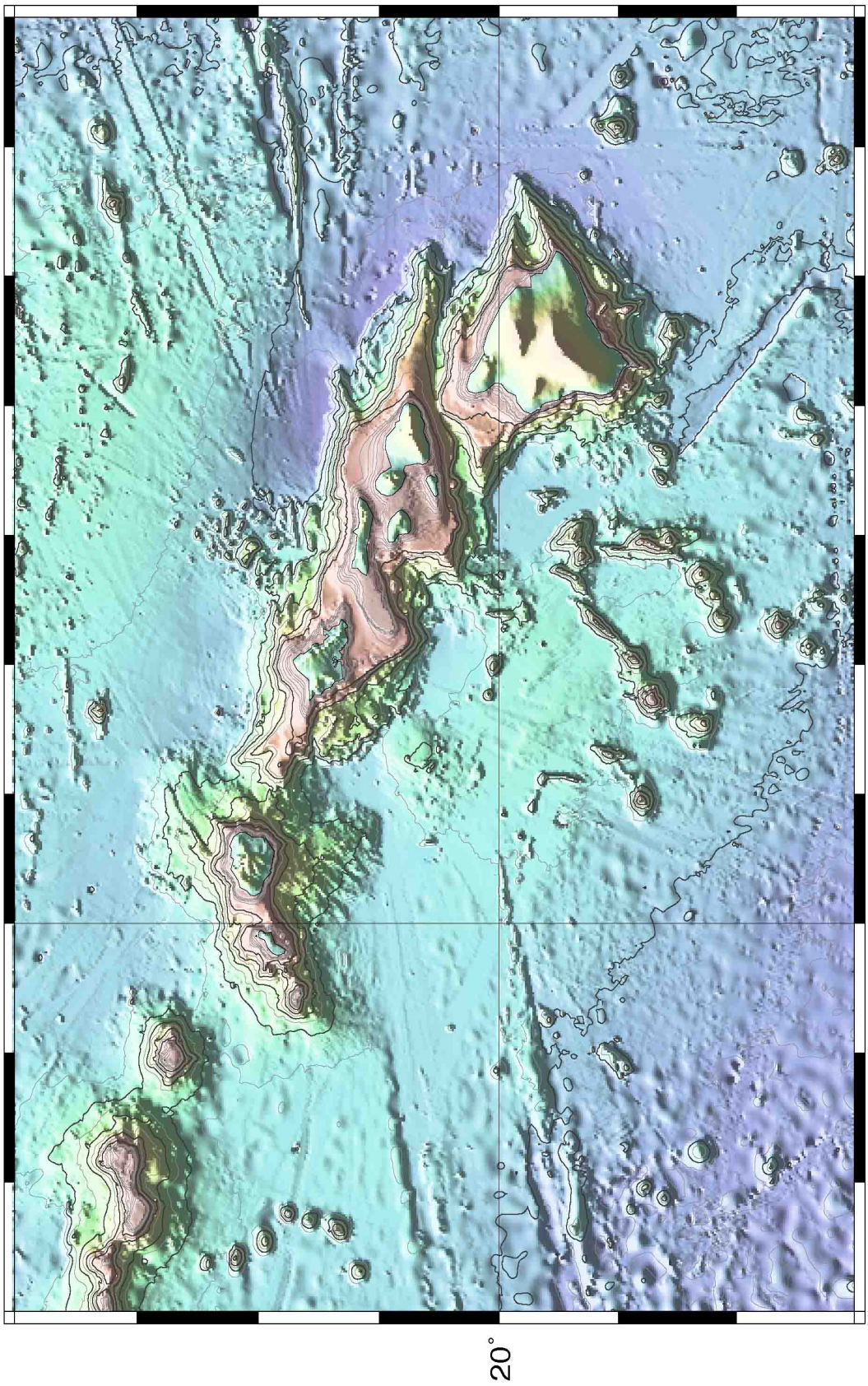

Figure 2-9: Figure 2-7, but without soundings.

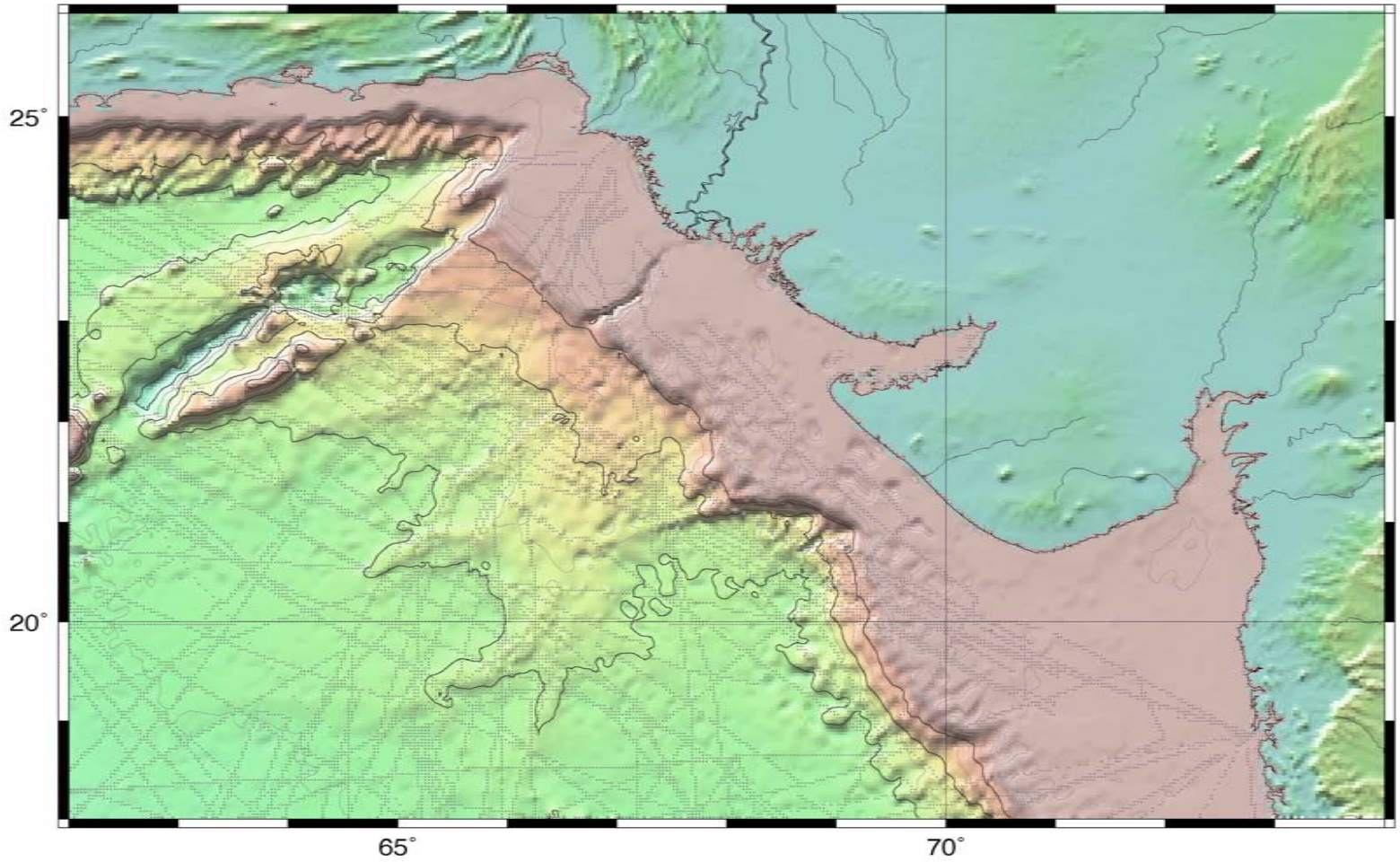

Figure 2-10: Arabian Sea near Karachi Pakistan from [Smith and Sandwell, 1997] global bathymetry.

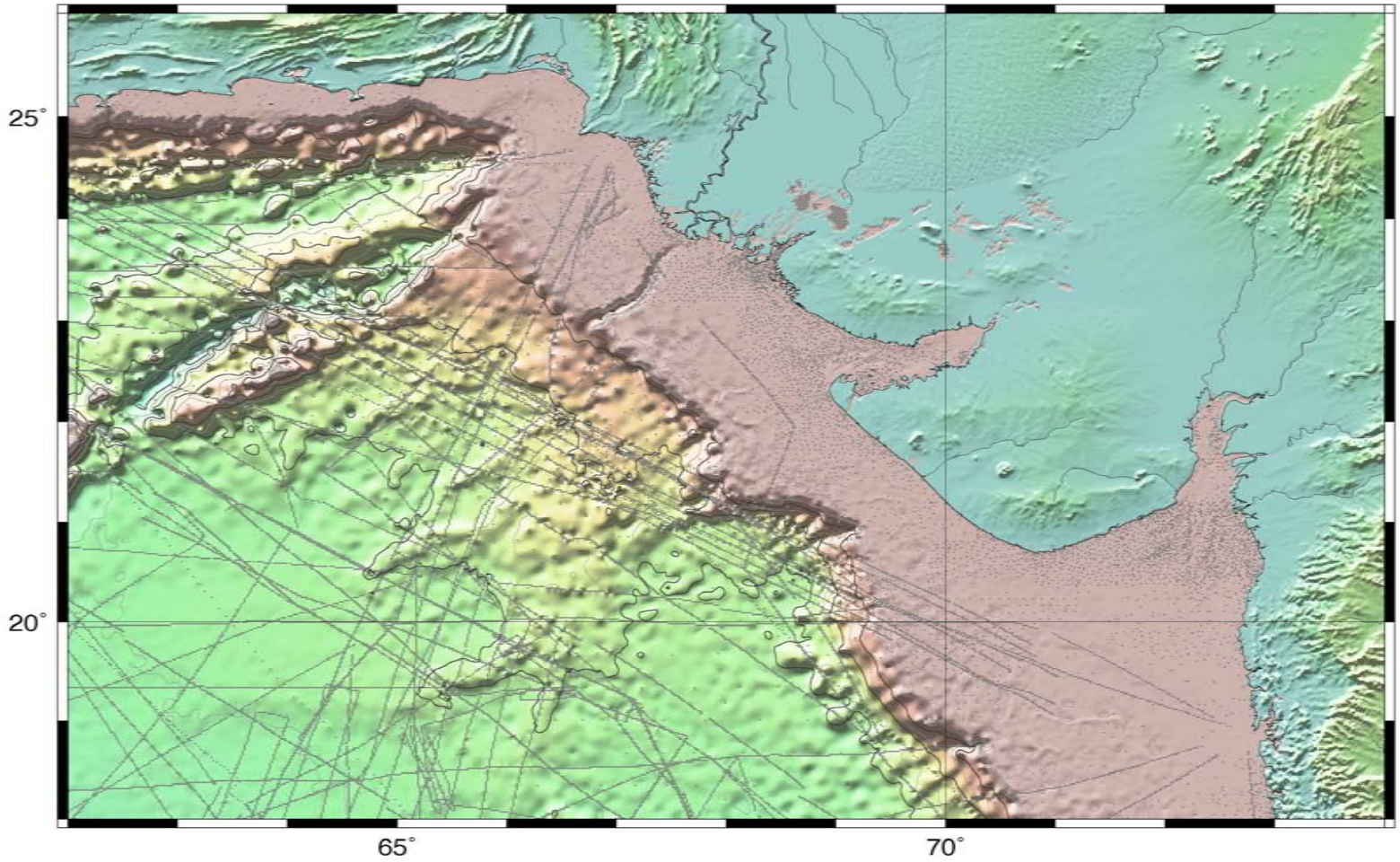

Figure 2-11: As Figure 2-9, but the global bathymetry presented here. Additional soundings on the continental margin in greatly improves the bathymetry.

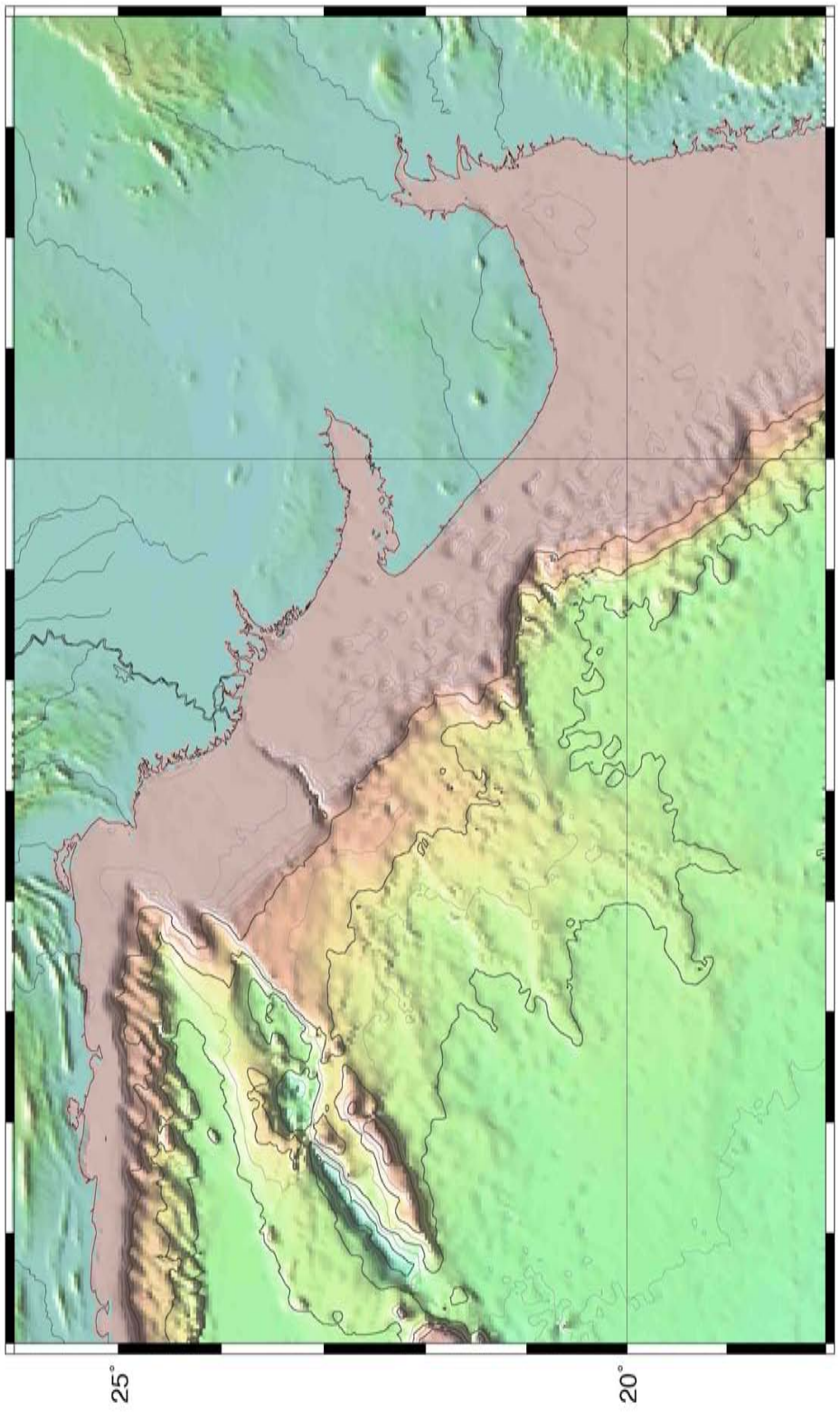

Figure 2-12: Figure 2-10, but without soundings.

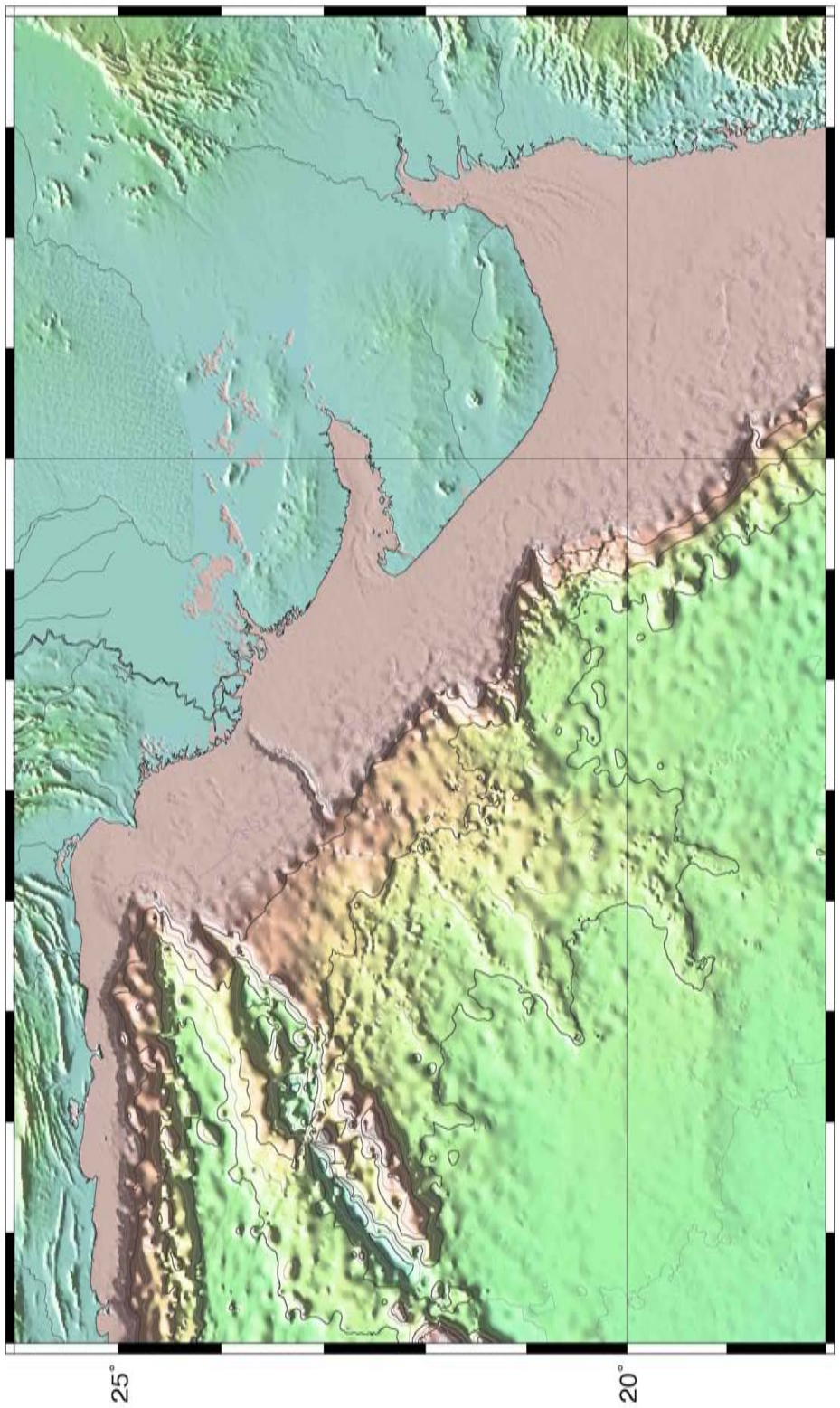

Figure 2-13: Figure 2-11, but without soundings.

3

Global Estimates of Seafloor Slope from Single-Beam Ship Soundings

3.1 ABSTRACT

Rough topography on the ocean floor is a source of ocean mixing which is of interest to both physical oceanography and climate science. Most mixing has been attributed to high slopes of the large-scale structures of the deep ocean floor such as seamounts, continental margins, and mid-ocean ridge axes. In this paper, we show the small-scale but ubiquitous abyssal hills and fracture zones dominate the global map of rough topography. Much of this rugged seafloor occurs in the Southern Ocean on the flanks of the Pacific-Antarctic Rise and Southwest Indian Ridge. We present our results as a global map of the mean slope of the ocean floor, and as a global map of the ocean floor above the M_2 critical slope. We compare our results to multi-beam and satellite bathymetry data to show that satellite bathymetry is not a valid proxy for multi-beam measurements, but edited single-beam sonar data are adequate to provide a global perspective on features with horizontal wavelengths as small as 2 km.

3.2 INTRODUCTION

In a classic paper, *Munk* [1966] assumed constant upwelling and estimated the eddy diffusivity needed to maintain the observed abyssal ocean stratification as well as the amount of energy needed to mix the abyssal ocean. The $O(10^{-4}$ $m^2/sec)$ diffusivity [*Munk*, 1966] predicted was not found experimentally [c.f. *Osborn*, 1980]. Eddy diffusivity is difficult to measure, but with the semi-empirical methods of *Osborn* [1980; 1972] and *Dillon* [1982], reliable experimental results were obtained. Recent measurements show that mixing is enhanced by orders of magnitude near rough topography [*Nash et al.*, 2007; *Polzin et al.*, 1997; *Toole et al.*, 1997]. *Munk and Wunsch* [1998] addressed the missing diffusivity in the mid ocean and the increased mixing over rough topography by proposing that tidal dissipation was a power source of mixing and mixing preferentially occurred when internal tides flowed across steep slopes. There is an extensive body of experimental, theoretical, and numerical research on the production of internal waves by the interaction of tidal currents with variable topography [cf. [*Garrett and Kunze*, 2007]. *Baines* [1982] examined the simple case of horizontal tidal excursions impinging on a uniform continental slope and found that for semidiurnal tides in a stably stratified layer, there is a critical slope where conversion of the barotropic tide is most efficient. In the deep ocean where the stratification is low, this critical slope ranges from 0.1 to 0.3 m/m so only very steep topography can generate internal waves in this simplified model. [*Llewellyn Smith and Young*, 2002] extended the model to show the shape of the topographic spectrum determines the amount of energy conversion in an ocean of finite depth with arbitrary stratification.

Satellite altimetry has been used to measure the global barotropic tide [*Kantha*, 1995], as well as the location and magnitude of its global dissipation [*Egbert and Ray*, 2000; 2001; 2003]. The global dissipation studies indicated that the approximately 1/3 of

the semi-diurnal barotropic tidal dissipation occurs in the deep oceans, apparently over the mid-ocean ridges (MOR) and seamounts. However, the dissipation maps do not have sufficient spatial resolution to provide a clear correlation with seafloor structures [*Egbert and Ray*, 2003]. The lack of resolution reflects the wide track spacing of Topex/Poseidon altimeter profiles (~150 km) as well as the subtlety and difficulty of the measurements presented in *Egbert and Ray* [2003].

In this paper, we present the global spatial distribution of seafloor slope and roughness in the abyss (depth > 2000 m). In particular, we focus on abyssal hills and fracture zones that extend over large parts of the ocean basins, especially on the lightly sedimented flanks of the slower spreading ridges. If, as proposed by *Ledwell* [2000], most of the tidal dissipation in the deep ocean occurs on abyssal hills, mapping their global distribution is important. We also show a significant fraction of seafloor (4.5%) has slope greater than the M_2 critical slope. Much of this super critical seafloor occurs in the Southern Ocean on the flanks of the Pacific-Antarctic Rise and Southwest Indian Ridge. These high-slope facets have either not been detected before, or have been grossly underestimated because satellite bathymetry [*Smith and Sandwell*, 1997] does not resolve features having horizontal scales less than 10 km.

3.3 GLOBAL ESTIMATE OF CRITICAL SLOPE

While we are considering a more complete spectral analysis of the sounding data, a great deal can be learned from a simple "critical slope" analysis. The internal tide literature *Baines* [1982] describes topography as being either super or sub critical. A well-known approximation for the critical slope of the topography is [*Baines*, 1982]

$$\alpha^2 \approx \tan^2(\theta_g) = \frac{(\omega^2 - f^2)}{(N^2 - \omega^2)} \qquad (1)$$

where θ_g is the angle between the group velocity vector and the horizon, ω is the frequency of internal wave (radian/sec) generated by the M_2 tide, f is the inertial frequency and N is the buoyancy frequency. For waves of given frequency (always M_2 in this paper) at given latitude the only unknown is the buoyancy frequency which depends on the density profile,

$$N^2 = \frac{-g}{\rho}\frac{\partial \rho}{\partial z} - \frac{g^2}{c^2} \approx \frac{-g}{\rho}\frac{\partial \rho_\theta}{\partial z} \qquad (2)$$

where z is the vertical coordinate, c is the speed of sound, ρ the in situ density, ρ_θ the potential density, and g is the acceleration of gravity (9.8 m/s^2) [*Knauss*, 1997].

A detailed global density profile is unavailable. We calculate an approximate buoyancy frequency profile using the CSIRO MATLAB routines [*Morgan and Pender*, 2003] at every depth and location in the 1˚ World Ocean Atlas (WOA) [*Conkright et al.*]. Noise in the WOA values of temperature and salinity made the calculated values of N^2 noisy and occasionally negative. To stabilize our estimate of N, we first removed negative values of N^2 and other obvious errors, and then followed *St Laurent and Garrett* [2002] by fitting N to an exponential function of depth.

$$\ln(N) = c_0 + c_1 z \qquad (3)$$

For depths that exceed the maximum depth in the WOA, we simply assumed N changes only slightly at abyssal depths, and used the deepest WOA depth at that location rather than extrapolate a fit to very noisy data. The calculated critical slope has at least two significant sources of error. First, the value of N is based on the WOA and which is an empirical data set with the usual potential for random and systematic errors. Secondly,

our N is an empirical fit to an exponential of depth [*St Laurent and Garrett*, 2002]; the truth is substantially more complex. As a result, our critical slope calculation is a semi-qualitative result.

To test the accuracy of our critical slope calculation we compared it to CTD data from two WOCE cruises. Appendix I is a comparison of our fit to the WOA data and WOCE CTD data along a meridian at 150 W between Alaska and Antarctica. We find good agreement between the critical slope estimates from these two independent data sets suggesting that the WOA data is adequate for this global analysis.

The global map of critical slope based on [*Conkright et al.*] is shown in Figure 1. The map extends only to +/- 72˚, so the M_2 turning latitudes at 75˚ are not visible. The latitudinal trend toward a critical slope of zero at those turning latitudes is apparent, as is the general decrease of N (increasing critical slope) with increasing depth. Low critical slope occurs on the shallow continental margins, the crests of seamounts such as the Hawaiian ridge, and along the mid-ocean ridges with depths between 2000-3000 m. There is a prominent asymmetry between the North and South Pacific, east-west asymmetries in the South Atlantic, across the equatorial East Pacific Rise, and across the Ninety-East Ridge in the Indian Ocean. This asymmetry is also seen in the WOCE CTD analysis provided in Appendix I.

3.4 SATELLITE BATHYMETRY GREATLY UNDERESTIMATES SEAFLOOR ROUGHNESS

The slope of the ocean floor depends on the length-scale of interest since, for example, individual pillow basalts can have vertical sides. The critical slope theory assumes that the length scale of the topography is greater than the tidal excursions of ~200 m [*Garrett and Kunze*, 2007]. A typical single beam echo sounder has a beam width

of ~15˚ so in the deep ocean (4000 m) it insonofies a zone about 1000 m across. Higher resolution (~200 m) is possible with modern multibeam systems but much of that data is collected at transit velocities, which limits the resolution to several hundred meters.

Three types of measurement systems are used to map the topography and roughness of the ocean floor. Single beam echo sounders, widely used since the 1960's, provide profile of depth from thousands of research cruises (Figure 2). While coverage is widespread, there are gaps as large as 200 km by 200 km, especially in the Southern Ocean. Multibeam echo sounding, available on most large research vessels since the mid 1990's, map 5-20 km wide swaths of seafloor at a horizontal resolution that depends on the depth of the water; 200-500 m at 4 km depth depending on ship speed and swath width. Ideally, the world's oceans should be exhaustively measured with multibeam bathymetry, but only a small percentage of the ocean floor has been so measured [*Smith and Sandwell*, 2004]. The third approach combines the sparse ship soundings with dense satellite-derived gravity anomalies to estimate depth and roughness [*Gille et al.*, 2000; *Smith and Sandwell*, 1997]. Satellite bathymetry can only resolve features with wavelengths between 20 and 160 km and misses most, if not all, of the small-scale roughness associated with the abyssal hill fabric. While none of these three measurement systems provides global coverage at the scales of interest (2 – 200 km), we show that the along-track analysis of the single beam provides an acceptable compromise between coverage and resolution if abyssal hills are assumed to be smoothly varying in slope over distances greater than a few hundred kilometers [*Goff*, 1991].

To assess the accuracy and resolution capabilities of each of the three systems, we compared multibeam, single beam, and satellite bathymetry along the track of an error-free, but otherwise typical cruise near the Atlantis Transform Fault on the Mid Atlantic Ridge (Figure 3). The multibeam data are from a 500-m grid provided by the Ridge Multibeam Synthesis project [*Carbotte*, 2004] and is considered in this paper to represent

the “true” depth. The single beam data were filtered and differentiated, as discussed below, to best match the multibeam slopes. Indeed the agreement between multibeam and single beam data is quite good for both depth and slope. In contrast the satellite bathymetry does not capture the smaller-scale topography associated with the abyssal hills. This is evident in the slope comparison where the *rms* slope calculated from satellite bathymetry (0.038 m/m rms) is much smaller than the slope derived from the multibeam and single beam systems (0.095 and 0.111 m/m *rms*). The inability of satellite bathymetry to accurately recover seafloor slope is illustrated in Figure 4, which shows a cumulative histogram of the absolute value of the slope for each of the three systems along the entire track line. Both sonar systems show that about 30% of the seafloor has slope greater than 0.1 m/m while the satellite bathymetry indicates only 2% of the seafloor of slope is greater than 0.1 m/m. This deficiency in the satellite bathymetry makes it unsuitable for quantifying seafloor slope due to abyssal hills.

To further assess the accuracy and resolution of the single beam data, we compared single beam slopes of the 43 ship tracks in the Atlantis Fracture Zone area (Figure 2c) to slopes derived from a multibeam grid available at 200 m, 500 m, and 1500 m spacing. As noted above the footprint of a single beam system in the deep ocean is ~1000 m but the along-track sampling is only 330 m at transit speed so the true along-track resolution is probably somewhere between these two values. These grids were compiled by the Ridge Multibeam Synthesis Project [*Carbotte*, 2004] and represent the best practices of the marine geology and geophysics community. It should be noted that there is a tradeoff between grid cell size and areal coverage so three resolutions are provided. While the 200-m resolution grids should provide the most accurate slope information, the coverage is much less complete than the 500-m grid. The 1500-m grid has the most complete coverage at the expense of lower resolution. To perform the slope comparison, the gradient of the multibeam grid was sampled along the trackline of the

single-beam profile and the along-track slope was computed as the dot product of this gradient vector with the ship direction vector. The *rms* of the multibeam slope was 0.14, 0.12, and .10 m/m respectively, clearly showing a loss of roughness as the grid resolution increased from 200-m to 1500-m. In addition to *rms*, we performed a robust regression analysis between co-located single beam profiles. A regression value greater than one indicates that the single-beam slope is overestimating the "true" seafloor slope or the multibeam grid is over-smoothed. The regression values for the 200-m and 500-m grids are close to one (1.04 and 1.09, respectively). In contrast, the slope of the single-beam data is 1.5 times greater than the slope derived from the 1500-m grid suggesting that the 1500-m grid is too smooth to fully capture seafloor slope at a wavelength of 2 km. These comparisons demonstrate that the along-track slope derived from a single-beam profile is similar in amplitude to the best multibeam grids at 200-m and 500-m resolution.

While single beam slope measurements are close to the multibeam "truth", they have not been analyzed previously because the archived data are contaminated by many error sources. There are three main types of problems with the single beam measurements. First, the depth soundings can be inaccurate due to "blunders", scale factor errors, and poor along-track sampling [*Smith*, 1993]. Second, older cruise data often contain large navigational errors that place soundings in the wrong location. While this is an issue for creating depth grids, navigation errors are not a problem for computing spatially averaged along-track slopes. Third, the coverage is non-uniform and the slope can only be computed along the track line of the ship. Track density is generally sparse in regions that are remote, have extreme weather, or are topographically uninteresting (Figure 2). In particular the abyssal plains and hills, (far from ports, mid-ocean ridges and other areas of geologic interest), are poorly sampled. Since bathymetry derived from gravity data became available in 1997, cruises have often been planned to avoid areas of smooth topography. As a result, recent sounding data have a potential sampling bias

toward rough seafloor that is difficult to quantify.

3.5 METHOD

The most challenging issue related to the single beam data is that slope can only be estimated along the track line of each cruise leg. In lightly sedimented areas, seafloor fabric is dominated by abyssal hills (Figure 2c) that are elongated in the direction of the fossil spreading ridge, because they were formed by ridge-parallel normal faulting and volcanism [*Goff*, 1991; *Goff and Smith*, 2003; *Macdonald and Luyendyk*, 1985; *Macdonald et al.*, 1996; *Smith*, 1998]. Because the abyssal hills have a preferred orientation, a single beam profile must be oriented perpendicular to the hill to measure the full magnitude of the seafloor gradient. This is illustrated in Figure 5 where we have plotted the slope along the track line of many cruises against the magnitude of the gradient vector derived from a 500-m multibeam grid. Theoretically, the along-track slope should be less than the gradient, but in this example, there are deviations reflecting the inconsistencies in the two types of data due to the inherent smoothing of the measurement as well as the smoothing related to gridding.

While the single beam profiles measure only the along-track component of seafloor slope, their coverage is much more complete than the coverage of the multibeam swaths so they provide a better sampling of the global seafloor slope. We can partly overcome the 1-D sampling of a 2-D topography by projecting the statistical properties of the seafloor gradient to the statistical properties of along track slope. Appendix II provides an analysis that demonstrates the magnitude of the gradient of a patch of sea floor is typically $\pi/2$ higher than the along-track slope measured by a ship having a randomly oriented trackline. The orientation of the ship tracks, with respect to the abyssal fabric, is sometimes, but not always, random. Seagoing expeditions not focused

on seafloor geology, or cruises in transit across the basins, sample the abyssal fabric in an essentially random direction. However, a cruise focused on geology and geophysics is typically preferentially oriented perpendicular or parallel to the abyssal fabric (e.g., Figure 2, bottom). Because of this possible sampling direction bias, we report mean slope without scaling up by $\pi/2$. This conservative approach understates the extent of supercritical seafloor.

3.6 DATA PROCESSING

The examples provided so far have used single beam data that are not contaminated by errors in depth or navigation. Approximately 1/3 of the 4900 cruise legs of single beam bathymetry data available from the GEODAS database [*NGDC*] have significant errors. These 1800 cruises have never been used in the global satellite bathymetry maps [*Smith and Sandwell*, 1997] even though, in many cases, the entire month-long set of depth soundings had only a few outliers. The automatic algorithm used to screen out obviously bad cruises generally failed to identify the occasional bad pings in good cruises because the types of errors are so diverse. Typical errors include: navigation errors, digitizing errors, typographical errors due to hand entry of older sounding, reporting the data in fathoms instead of meters, incorrect sound speed measurements, and even computer errors in reading punch cards [*Smith*, 1993]. Just one bad section of a cruise in an isolated region introduces a seafloor topographic feature that does not exist and the entire cruise is rejected.

About 5000 cruises of single beam soundings collected over the past 40 years and archived at the National Geophysical Data Center [*NGDC*] have been hand edited by comparing measured depth to satellite bathymetry (i.e., based on gravity only). These data will be combined with multibeam data to refine the global satellite bathymetry

grid [*Smith and Sandwell*, 1997] and create a new global grid at 1 km resolution. This involved the development of a graphical user interface program consisting of three linked windows, the ship track, the along track profile, and a scatter diagram of altimetric versus measured depth. Typical *rms* differences between the measured and satellite bathymetry are 250 m. We expect the *rms* errors in the soundings to be less than 25 m [*Smith*, 1993] so most of the bad soundings are obvious outliers. The analyst scans the profile data for large deviations from the satellite bathymetry (typically > 500 m) and flags these data as being suspect. The edited cruise is returned to the database with the suspect data flagged. Using this tool, we have edited the approximately 30 million pings from the GEODAS database.

These clean data were then low pass filtered and differentiated along-track to estimate seafloor slope as discussed below using the software tools in GMT [Wessel and Smith, 1995]. The ship track profiles were pre-filtered with a Gaussian low pass filter having a 0.5 gain at a wavelength of 2 km. The 2-km filter is partly motivated by the expected beam width of single beam sonar (~1 km) in the deep ocean [Smith, 2005]. Ship track data are unequally spaced; e.g., the ship speed changes, but the ping rate is relatively uniform. Moreover, the spacing of the older hand-digitized data is based on the seafloor features. For example, flat abyssal plains sometimes have 4-km spacing between soundings because the human digitizer determined that a finer spacing was unnecessary. This uneven and sometimes large spacing does not strictly support a 2-km wavelength resolution. We selected this resolution as a compromise because the widely spaced older soundings presumably would have a smaller spacing if the human digitizer felt it was needed to capture the actual seafloor slope. After low pass filtering, the data were differentiated along-track at a minimum interval of 1/4 the wavelength of the low-pass filter (500 m). More complex signal processing is not needed when the ship track data is correctly edited.

The calculation of the fraction of seafloor above critical slope discussed below was done in three steps in order to minimize the bias due to the uneven distribution of ship soundings. First, we created two 0.1˚ longitude by 0.1˚ latitude grids - one consisting of the total number of slope estimates in each grid cell and a second consisting of the number of slope estimates (absolute value) that exceed the critical slope in each grid cell. Second, these two grids were low pass filtered with a radial Gaussian filter (σ=10km) to determine the number of slopes per 628 km^2; the integrated area under a radial Gaussian is $2\pi\sigma^2$. Third, the fraction of seafloor with slope above the critical slope was computed as the ratio of the two grids. Areas with less than one ping per 100 km^2 were not used to avoid taking the ratio of very small numbers. For display purposes, the fraction of seafloor above critical slope is median filtered and interpolated onto a 1˚ grid (Figure 7a). This process combines the information in Figures 5 and 6.

3.7 GLOBAL MEASUREMENT OF SEA FLOOR ROUGHNESS

The global map of spatially averaged seafloor slope is shown in Figure 6. Along-track slopes were binned in a 0.25˚ longitude by 0.2˚ latitude intermediate grid and the mean slope was calculated for each bin. The binning is done to reduce the bias due to uneven sampling by the ship soundings. In particular, the ridge axes are sampled much more densely than the abyssal plains. We find that seafloor slope varies more than an order of magnitude throughout the deep oceans and depends on a combination of tectonic and sedimentary processes. Large-scale features (> 40 km) such as continental margins, ridge axes, fracture zones, trenches, and seamounts are sometimes associated with slope greater than 0.05. These large-scale features are well resolved in bathymetry derived from satellite-derived gravity anomalies and sparse ship soundings [*Smith and Sandwell*,

1997]. Such maps have been band-pass filtered between 20 and 160 km wavelength to reveal the slope and roughness of the seafloor and to relate these bottom characteristics to mesoscale variability [*Gille et al.*, 2000] and ocean mixing [*Jayne and St Laurent*, 2001]. Using only ship soundings, we find that the global mean slope map is dominated by the distribution of the smaller-scale abyssal hill topography and fracture zones. Abyssal hills are generated at mid-ocean ridges by a combination of volcanism and normal faulting [*Cannat et al.*, 2006; *Lonsdale*, 1977; *Macdonald and Luyendyk*, 1985]. The amplitude and wavelength of abyssal hills depends strongly on the rate of seafloor spreading [*Goff*, 1991; *Goff et al.*, 2004; *Kunze and Llewellyn Smith*, 2004] that also controls the morphology of the spreading ridge axis where they were formed [*Canuto et al.*, 2004; *Macdonald*, 1982; *Macdonald et al.*, 1988; *Menard*, 1967; *Small and Sandwell*, 1992]. On older seafloor, a thick layer of sediment often covers the abyssal fabric. Sedimented seafloor can be extremely flat at the scale of abyssal hills. In summary, there are basin-scale variations in seafloor slope that are well explained in terms of variations in seafloor spreading rate and the thickness of the sediments. These spatial variations in slope occur over distances greater than a few hundred kilometers [*Goff and Jordan*, 1989] so the sparse track sampling in the Southern Ocean (~40 km track spacing) is adequate for characterizing global seafloor slope.

3.8 FRACTION OF SEAFLOOR ABOVE CRITICAL SLOPE

Given the slope along each ship track and the critical slope interpolated to the same location we calculate the fraction of seafloor having slope above the critical slope. This calculation is allows us to estimate the total area of super critical seafloor. It is also useful because it at least partially addresses the issue of mixing hot spots. [*Nash et al.*, 2007] suggest that mixing in the deep ocean is localized in a few small areas. Therefore,

an area's potential for mixing may not be the average critical slope, but the fraction of the area that is super critical.

For comparison, we performed a similar analysis using the global 2-minute grid of *Smith and Sandwell* [1997] (Figure 7b). Since the full gradient of the *Smith and Sandwell* [1997] grid was calculated, we would expect slopes from the gradient of *Smith and Sandwell* [1997] to be $\pi/2$ times greater than single beam slopes, and thus the fraction of seafloor above the critical slope should be $\pi/2$ larger. Instead, we find the super-critical fraction of seafloor for [*Smith and Sandwell*, 1997] to be substantially less than that derived from the single beam soundings. This is because, as discussed above, satellite bathymetry does not capture the full magnitude of the seafloor gradient because it only resolves wavelengths > 20 km.

The ship data and the satellite bathymetry grid have similar super-critical seafloor fraction for the large-scale structures of the ocean basins such as continental margins, ridge axes, ocean trenches and back-arc volcanoes and intra-plate island chains such as Hawaii. This is expected because these large-scale features are well resolved in the satellite bathymetry grid. However, there are major differences (Figure 7a and 7b) on the flanks of ridges especially in the Southern Ocean where the critical slope at the bottom of the ocean is less than 0.2 m/m.

To quantify this observation we plot the area of seafloor with supercritical slope versus ocean depth (Figure 8 - thick line). Seafloor spreading ridges lie at depths between 2000 m and 3000 m. The ridge flanks lie at depths between 3000 m and 4500 m. It is clear that the fraction of supercritical seafloor on the ridge flanks is larger than the fraction of supercritical seafloor on the ridge axes. A similar analysis using satellite bathymetry arrives at just the opposite conclusion and suggests that the ridge axes are more important than the ridge flanks. Indeed the total fraction of supercritical seafloor in the deep ocean (> 2000 m deep) is 4.5% based on the single beam data and only 1.5%

based on the satellite bathymetry. These comparisons suggests that calculations based on slopes of the [*Smith and Sandwell*, 1997] grid are substantially underestimating the area of super critical seafloor, and it's location.

3.9 DISCUSSION AND CONCLUSIONS

We restrict our discussion to the deeper ocean areas (> 2000 m) where abyssal hills dominate the seafloor slope, and where we expect that spatial variations in slope and critical slope will be smooth relative to the characteristic spacing of the ship profiles. Our estimate of the fraction of seafloor above critical slope shows some obvious global patterns that deserve comment. The west flank of the southern mid-Atlantic Ridge is prominent, but areas of rough seafloor in the Southern Ocean dominate the fraction of seafloor above critical. In particular, the flanks of the Southwest Indian Ridge and the flanks of the Southeast Indian Ridge, especially in the Australian-Antarctic Discordant Zone (90˚-160˚E) are prominent as are the flanks of the Pacific-Antarctic Rise, and the flanks of the Scotia Sea Spreading Centers (50˚-60˚S, 75˚-30˚W). The presence of so much super critical topography near the Antarctic Circumpolar Current (ACC) is striking. We speculate that the ACC may be sweeping the sediment off the ridge flanks, creating an area of rough topography in a strong current.

Our conclusions are: 1) The 40-year archive of single beam bathymetry provides a global perspective on the slope and roughness of the seafloor although the data have some significant shortcomings. First, the original data are highly heterogeneous because they were collected with multiple generations of echo sounding and navigation technology and were digitized and assembled by hundreds of scientists on tens of research vessels. By visually editing 4900 cruises assembled at NGDC, we were able to extract seafloor slope and roughness information for wavelengths greater than 2 km and confirmed the results

in small areas where complete multibeam coverage is available. A second problem with the single beam bathymetry data is that the seafloor slope can only be estimated along the trackline of the ship, which is usually not in the direction of maximum seafloor gradient. Assuming the direction of the ship tracks is random with respect to the abyssal hill fabric, we show that, on average, the along-track slope will be $2/\pi$ less than the magnitude of the gradient. We use the along-track slope estimate as a proxy for seafloor slope knowing it represents a lower bound on the actual slope.

2) The critical slope at the bottom of the ocean associated with conversion of the barotropic M_2 tide was estimated from a global compilation of temperature and salinity measurements [*Conkright et al.*]. Sparse measurements, especially in the Southern Ocean, prevent the construction of a spatially detailed map of critical slope. We argue that in the deep ocean (< 2000 m) spatial variations in temperature and salinity will be small so this global representation may be qualitatively correct. Interpolating this critical slope map to the locations of the measured seafloor slope, we estimate the fraction of seafloor with slope that exceeds the critical value. In contrast to previous studies based on altimetry-derived depth, we find large areas that have slope exceeding the critical value.

3) Our results are consistent with previous studies that show a high fraction of seafloor above critical slope along the mid-Atlantic ridge and Hawaiian Chain but suggest that barotropic tidal conversion dominantly occurs in the Southern Ocean where sediments are thin and the abyssal hills have relatively high amplitude because they formed at a fossil spreading rate less than the threshold value of 70 mm/yr. The global analysis shows that the largest areas of super-critical slope are on the flanks of the seafloor spreading ridges. The largest areas of super critical slope are the Southwest Indian Ridge flanks, the Southeast Indian Ridge flanks, the southern Mid-Atlantic Ridge flanks, the Scotia Ridge, and most importantly, the Pacific Antarctic Rise away from the ridge axis.

3.10 APPENDIX I - COMPARISON OF CRITICAL SLOPE FROM WOCE P16 CTD CASTS AND NUMERICAL FITS TO WOA [2001]

The global map of critical slope (Figure 1) shows obvious hemispherical variation with the lower critical slope in the South Pacific than North Pacific. To verify this hemispherical asymmetry, we compared our numerical fit of World Ocean Atlas (WOA) 2001 data [*Conkright et al.*] to the critical slope calculated from Salinity, Temperature, and Pressure data (commonly referred to as CTD) from two World Ocean Circulation Experiment (WOCE) repeat cruises in 2005/06. These cruises revisited the "P16" line in the Pacific that runs along longitude 150W from Antarctica to Alaska with a CTD cast taken at least once every degree of latitude from 72S to 56N. These particular data were not used in the WOA 2001 analysis [*Conkright et al.*]. The 2005/2006 cruises had modern navigation and CTD instrumentation and they sampled the entire water column from surface to approximately 10m above the bottom. A typical CTD rosette has redundant sensors that are calibrated on shore and against each other on each station. The noise present in the data is on the order of 1 part per thousand or better. This level of instrument noise is inconsequential since the microstructure of the water column dominates the instrumentation noise. The standard deviation of N due to the microstructure was typically 0.25 *cph* in the deepest bin, which is a large fraction of the total estimate of N so this environmental noise dominates. At one station in the North Pacific at 28N, either an overturn was observed at the bottom, or there was a data error large enough to create a negative N^2. As in the cases of computing N from the WOA, this value of N and the critical slope are both set to zero.

The CTD data from 190 casts were processed into critical slope at the bottom of the ocean as follows. The "exchange" data in comma separated value (CSV) format from

the 2005 repeat of the P16S line on cruise 33RR200501, and the 2006 repeat of P16N from cruise 325020060213 were down loaded from the CLIVAR & Carbon Hydrography Office (CCHDO) website [*Swift*] and processed using MATLAB software [*MathWorks*, 2007]. For each of the depth casts, the CTD were processed using the CSIRO algorithm [*Morgan and Pender*, 2003] of the UNESCO seawater equation of state. The data for each cast were then binned and averaged at the WOA standard depths. The deepest bin in each P16 station was compared to the numerical fit from the WOA 2001 data [*Conkright et al.*]. The maximum depth of the water at P16 stations is rarely more than 100 m deeper than the maximum standard depth in the WOA.

Estimates of critical slope from the WOA and P16 are plotted in Figure 9 and show good agreement. Both estimates have an unknown uncertainty that is dominated by true fluctuations in density gradient. Therefore we performed a robust regression [*Laws*, 1997] using a "bisquare" weighting function in the MATLAB robustfit function where the model was constrained to go through the origin. Our calculation of critical slope using the WOA is slightly smaller than the experimental data (0.958 +/- 0.085), but it is within 5 percent of the experimental result and is consistent with a slope of one. The linear correlation is 0.497. The WOA data also show some anomalously high slopes that are due to underestimating the density gradient. Considering that the microstructure of N in the experimental data is approximately +/- 50%, we feel our use of a fit to the WOA to estimate global critical slope is justified.

Given this level of agreement we believe the north-south asymmetry in critical slope, shown in Figure 1, is real. Along this line of longitude the asymmetry is to be expected because of the Pacific basin in the northern hemisphere is generally 1-2 km deeper than the flank of the Pacific Antarctic Rise in the southern hemisphere and deeper ocean tends to be more stratified than shallower ocean. In conclusion, a critical slope calculated from WOA is error prone, but in good agreement with the more accurate CTD

data.

3.11 APPENDIX II - STATISTICAL RELATIONSHIP BETWEEN SLOPE AND GRADIENT

Assume the abyssal seafloor away from isolated seamounts and other distinct features is a stationary and ergodic function [*Bendat and Piersol*, 2000]. The gradient of a randomly oriented facet of sea floor is a random vector [*Goff*, 1991.]. Our objective is to describe the statistical properties of the gradient vector as well as to relate this to the statistical properties of the slope vector. Following [*Goff*, 1991], assume the *x*- and *y*-components of the gradient are independent, zero mean, and normally distributed with identical variance σ^2. As discussed by Freilich [1997], the histogram of the magnitude of this random vector is a Rayleigh distribution ($x > 0$)

$$f_{\text{Rayleigh}}(x;\sigma) = \frac{x}{\sigma^2}\exp\left(\frac{-x^2}{2\sigma^2}\right) \qquad \text{(A1)}$$

The mean value of the gradient *g* is

$$\bar{g} = \int_{g=0}^{\infty} g \cdot f(g;\sigma)dg = \sigma\sqrt{\frac{\pi}{2}} \qquad \text{(A2)}$$

Given this statistical model for seafloor slope we can relate the probability distribution of along-track slope to the Rayleigh distribution of gradient. Consider a tilted facet of seafloor oriented at an azimuth of ϕ with respect to the track line of the ship. The measured slope of the seafloor is always less than or equal to the magnitude of the gradient and it is given by $s = g\cos\phi$. The distribution for along track slope is related to the probability distribution for gradient by

$$f(s;\phi,\sigma) = f_{\text{Rayleigh}}(s/\cos\phi;\sigma)\left|\frac{\partial g}{\partial s}\right| = \frac{s}{\sigma^2\cos^2\phi}\exp\left(\frac{-s^2}{2\sigma^2\cos^2\phi}\right). \qquad \text{(A3)}$$

We need to integrate over all azimuths and normalize by 2π to obtain the distribution for a randomly oriented facet.

$$f(s;\sigma) = \frac{1}{2\pi}\int_0^{2\pi} f(s;\phi,\sigma)\,d\phi = \sqrt{\frac{2}{\pi\sigma^2}}\exp\left(\frac{-s^2}{2\sigma^2}\right) \qquad \text{(A4)}$$

The Rayleigh distribution describing the gradient maps to a Gaussian distribution describing the along track slope. An example of theoretical gradient and slope distribution functions are shown in Figure 10 along with the histograms of observed gradient and slope shown in Figure 5. While there are discrepancies between the actual and model distribution functions, these simple ideas provide an approximate basis for deriving seafloor gradient information from along-track slope profiles. In particular, it is interesting to relate the mean along track slope to the mean gradient, ($s > 0$)

$$\bar{s} = \int_0^{\infty} s\cdot f(s;\sigma)ds = \sigma\sqrt{\frac{2}{\pi}} = \frac{2}{\pi}\bar{g}. \qquad \text{(A5)}$$

This relationship suggests the mean value of slope measured along a ship track is lower than the gradient by a factor of $2/\pi$ (64%). In this paper, we compute mean slope along ship tracks, and expect that the seafloor gradient is usually larger.

3.12 ACKNOWLEDGEMENTS

This paper benefited greatly from discussions with Walter Munk, Stefan Llewellyn Smith, Shaun Johnston, Sarah Gille, and Jennifer MacKinnon. Scott Nelson of UCSD edited the ship data with an astonishing rapidity and accuracy. We thank the

associate editor James Richman and the two reviewers for their many suggestions for improving the manuscript. We also thank Walter Munk for originally proposing this study in 1999 using satellite bathymetry. That preliminary comparison suggested (incorrectly) that the abyssal plains were not important in deep ocean mixing. The results were not published because we speculated that the slope of the seafloor from satellite bathymetry greatly underestimates the true seafloor slope. It has taken 8 years to go back, look at the raw sounding data, and arrive at a more accurate assessment. This research was supported by the Office of Naval Research (N00014-06-1-0140) and the National Science Foundation (OCE-0326707).

The text and figures from chapter 3 are being prepared for publication in JGR Oceans as Becker, J. J. and Sandwell, Global Estimates of Sea floor Slope from Single-Beam Ship Soundings The dissertation author was the primary researcher and author of the submitted work. The coauthor directed and supervised that research, which forms the basis for this chapter.

3.13 REFERENCES

Baines, P. G. (1982), On Internal Tide Generation Models, *Deep-Sea Research Part a-Oceanographic Research Papers*, *29*(3), 307-338.

Bendat, J. S., and A. G. Piersol (2000), *Measurement and analysis of random data*, Third ed., Wiley, New York.

Cannat, M., et al. (2006), Modes of seafloor generation at a melt-poor ultraslow-spreading ridge, *Geology*, *34*(7), 605-608.

Canuto, V. M., et al. (2004), Latitude-dependent vertical mixing and the tropical thermocline in a global OGCM, *Geophysical Research Letters*, *31*(16).

Carbotte, S. M. (2004), New Integrated Data Management System for Ridge2000 and MARGINS Research, *Eos*, *85*(51).

Conkright, M. E., et al. (12 Sep. 2007). WORLD OCEAN ATLAS 2001. http://www.nodc.noaa.gov/OC5/WOA01/pr_woa01.html (2 Jan. 2008).

Dillon, T. M. (1982), Vertical Overturns - a Comparison of Thorpe and Ozmidov Length Scales, *Journal of Geophysical Research-Oceans and Atmospheres*, *87*(NC12), 9601-9613.

Egbert, G. D., and R. D. Ray (2000), Significant dissipation of tidal energy in the deep ocean inferred from satellite altimeter data, *Nature*, *405*(6788), 775-778.

Egbert, G. D., and R. D. Ray (2001), Estimates of M-2 tidal energy dissipation from TOPEX/Poseidon altimeter data, *Journal of Geophysical Research-Oceans*, *106*(C10), 22475-22502.

Egbert, G. D., and R. D. Ray (2003), Semi-diurnal and diurnal tidal dissipation from TOPEX/Poseidon altimetry, *Geophysical Research Letters*, *30*(17), -.

Freilich, M. H. (1997), Validation of vector magnitude datasets: Effects of random component errors, *Journal of Atmospheric and Oceanic Technology*, *14*(3), 695-703.

Garrett, C., and E. Kunze (2007), Internal tide generation in the deep ocean, *Annual Review of Fluid Mechanics*, *39*, 57-87.

Gille, S. T., et al. (2000), Global correlation of mesoscale ocean variability with seafloor roughness from satellite altimetry, *Geophysical Research Letters*, *27*(9), 1251-1254.

Goff, J. A., and T. H. Jordan (1989), Stochastic Modeling of Seafloor Morphology - a Parameterized Gaussian Model, *Geophysical Research Letters*, *16*(1), 45-48.

Goff, J. A. (1991), A Global and Regional Stochastic-Analysis of near-Ridge Abyssal Hill Morphology, *Journal of Geophysical Research-Solid Earth*, *96*(B13), 21713-21737.

Goff, J. A., and W. H. F. Smith (2003), A correspondence of altimetric gravity texture to abyssal hill morphology along the flanks of the Southeast Indian Ridge, *Geophysical Research Letters*, *30*(24), -.

Goff, J. A., et al. (2004), The Contributions of Abyssal Hill Morphology and Noise to Altimetric Gravity Fabric, *Oceanography*, *17*(1), 24-37.

Jayne, S. R., and L. C. St Laurent (2001), Parameterizing tidal dissipation over rough topography, *Geophysical Research Letters*, *28*(5), 811-814.

Kantha, L. H. (1995), Barotropic tides in the global oceans from a nonlinear tidal model assimilating altimetric tides. 1. Model description and results, *Journal of Geophysical Research*, *100*(C12), 25283-25308.

Knauss, J. A. (1997), *Introduction to physical oceanography*, 2nd ed., 309 pp., Prentice Hall, Upper Saddle River, N.J.

Kunze, E., and S. G. Llewellyn Smith (2004), The Role of Small-Scale Topography in Turbulent Mixing of the Global Ocean, *OCEANOGRAPHY*, *17*(1), 55.

Laws, E. (1997), *Mathematical Methods for Oceanographers: An Introduction*, 343 pp., John Wiley, New York.

Ledwell, J. R., et al. (2000), Evidence for enhanced mixing over rough topography in the abyssal ocean, *Nature*, *403*(6766), 179-182.

Llewellyn Smith, S. G., and W. R. Young (2002), Conversion of the barotropic tide, *Journal of Physical Oceanography*, *32*(5), 1554-1566.

Lonsdale, P. (1977), Deep-Tow Observations at Mounds Abyssal Hydrothermal Field, Galapagos Rift, *Earth and Planetary Science Letters*, *36*(1), 92-110.

Macdonald, K. C. (1982), Mid-Ocean Ridges - Fine Scale Tectonic, Volcanic and Hydrothermal Processes within the Plate Boundary Zone, *Annual Review of Earth and Planetary Sciences*, *10*, 155-190.

Macdonald, K. C., and B. P. Luyendyk (1985), Investigation of Faulting and Abyssal Hill Formation on the Flanks of the East Pacific Rise (21-Degrees-N) Using Alvin, *Marine Geophysical Researches*, *7*(4), 515-535.

Macdonald, K. C., et al. (1988), A New View of the Mid-Ocean Ridge from the Behavior of Ridge-Axis Discontinuities, *Nature*, *335*(6187), 217-225.

Macdonald, K. C., et al. (1996), Volcanic growth faults and the origin of Pacific abyssal hills, *Nature*, *380*(6570), 125-129.

MathWorks, T. (2007), MATLAB, edited, The MathWorks, Natick, MA.

Menard, H. W. (1967), Sea Floor Spreading Topography and Second Layer, *Science*, *157*(3791), 923-&.

Morgan, P., and L. Pender (2003), SEAWATER A Library of MATLAB Computational Routines for the Properties of Seawater, edited, CSIRO Marine Research.

Munk, W. (1966), Abyssal Recipes, *Deep-Sea Research Part I-Oceanographic Research Papers*, *13*, 707-730.

Munk, W., and C. Wunsch (1998), Abyssal recipes II: energetics of tidal and wind mixing, *Deep-Sea Research Part I-Oceanographic Research Papers*, *45*(12), 1977-2010.

Nash, J. D., et al. (2007), Hotspots of deep ocean mixing on the Oregon continental slope, *Geophysical Research Letters*, *34*(1), -.

NGDC (11 Jan. 2006). GEODAS Search Criteria Selection. http://ftp.ngdc.noaa.gov/mgg/gdas/gd_cri.Html (2 Jan. 2008).

Osborn, T. R. (1980), Estimates of the Local-Rate of Vertical Diffusion from Dissipation Measurements, *Journal of Physical Oceanography*, *10*(1), 83-89.

Osborn, T. R., and C. S. Cox (1972), Oceanic fine structure, *Geophys. Fluid Dyn.*, *3*(321–345).

Polzin, K. L., et al. (1997), Spatial variability of turbulent mixing in the abyssal ocean, *Science*, *276*(5309), 93-96.

Small, C., and D. T. Sandwell (1992), An Analysis of Ridge Axis Gravity Roughness and

Spreading Rate, *Journal of Geophysical Research-Solid Earth*, *97*(B3), 3235-3245.

Smith, W. H. F. (1993), On the Accuracy of Digital Bathymetric Data, *Journal of Geophysical Research-Solid Earth*, *98*(B6), 9591-9603

.

Smith, W. H. F., and D. T. Sandwell (1997), Global sea floor topography from satellite altimetry and ship depth soundings, *Science*, *277*(5334), 1956-1962.

Smith, W. H. F. (1998), Seafloor Tectonic Fabric From Satellite Altimetry, *Annual Review of Earth and Planetary Sciences*, *26*(1), 697-747.

Smith, W. H. F., and D. T. Sandwell (2004), Conventional Bathymetry, Bathymetry from Space, and Geodetic Altimetry *Oceanography*, *17*(1), 8-23.

Smith, W. H. F. (2005), Personal Communication, edited.

St Laurent, L., and C. Garrett (2002), The role of internal tides in mixing the deep ocean, *Journal of Physical Oceanography*, *32*(10), 2882-2899.

Swift, J. (2 Jan. 2008). CLIVAR & Carbon Hydrographic Data Office. http://cchdo.ucsd.edu (2 Jan. 2008).

Toole, J. M., et al. (1997), Near-boundary mixing above the flanks of a midlatitude seamount, *Journal of Geophysical Research-Oceans*, *102*(C1), 947-959.

Wessel, P., and W. H. F. Smith (1995), New Version of the Generic Mapping Tools Released, *EOS*.

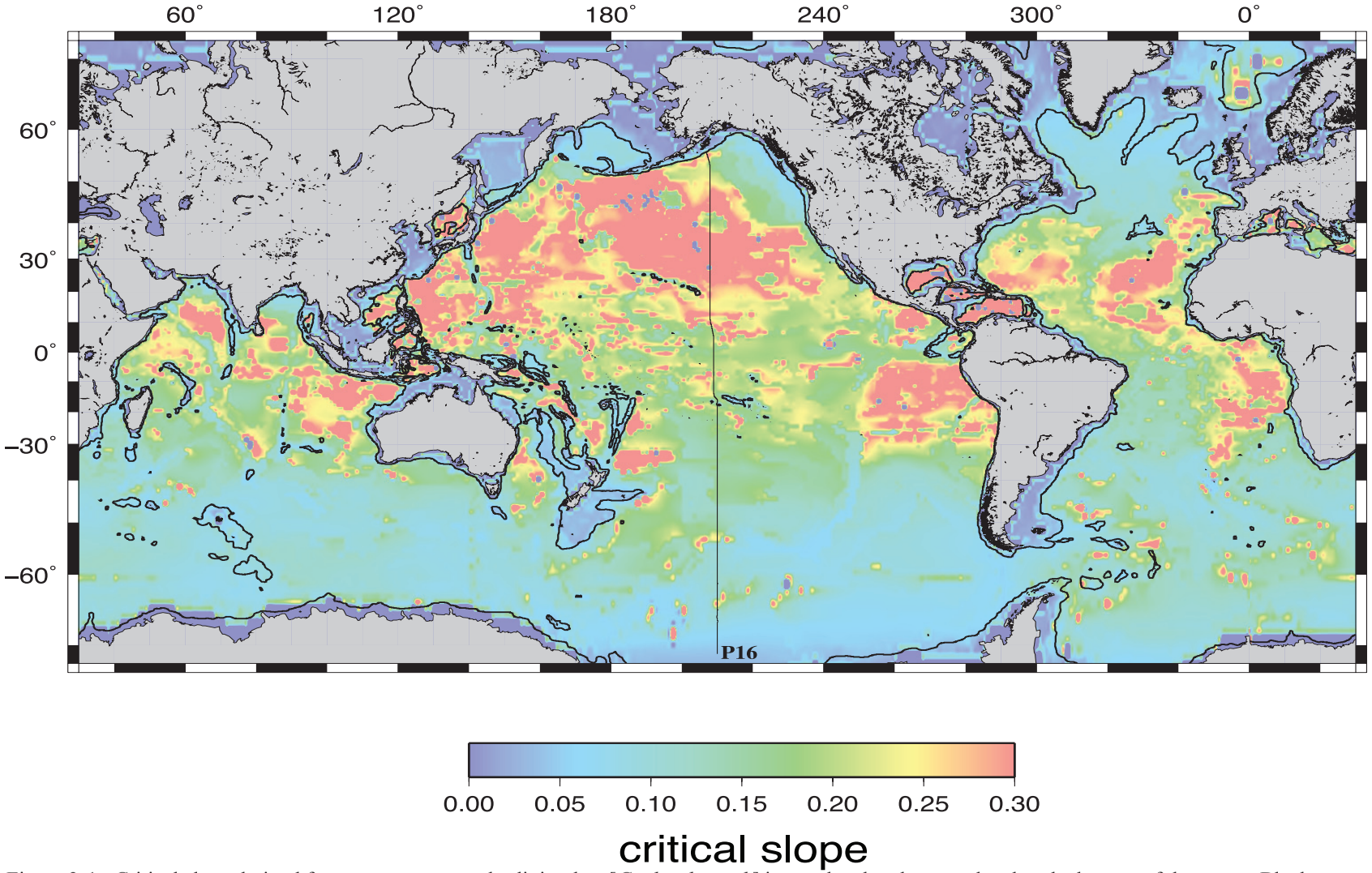

Figure 3-1: Critical slope derived from temperature and salinity data [*Conkright et al.*] interpolated and extrapolated to the bottom of the ocean. Black contour marks 3000 m depth. The WOCE P16 line along 150W is also shown.

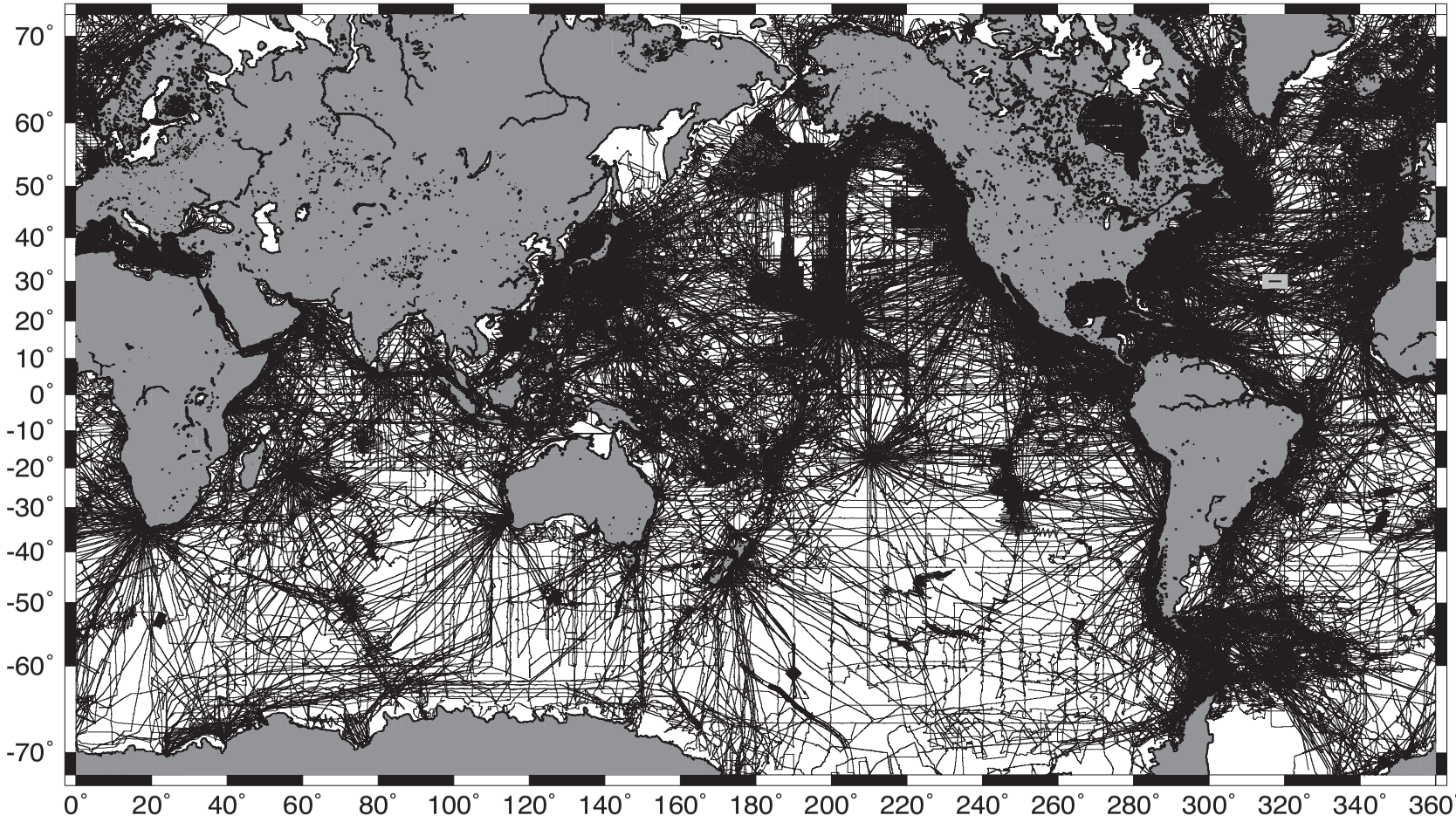

Figure 3-2: Distribution of single beam depth profiles from 4900 cruises collected over the past 40 years and archived at the National Geophysical Data Center. We have hand-edited these data to remove blunders and outliers.

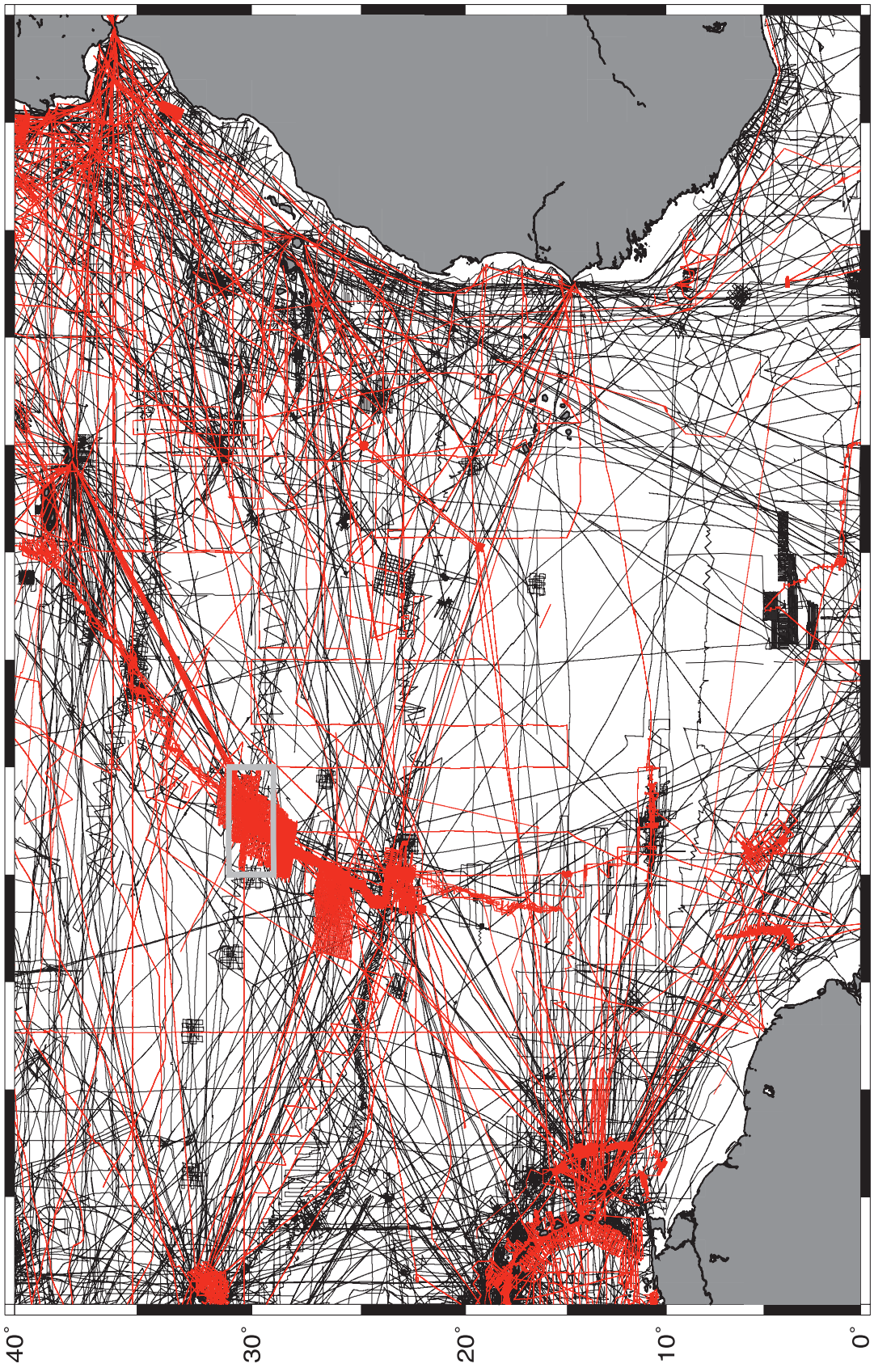

Figure 3-3: distribution of single and multi-beam echo soundings in the North Atlantic

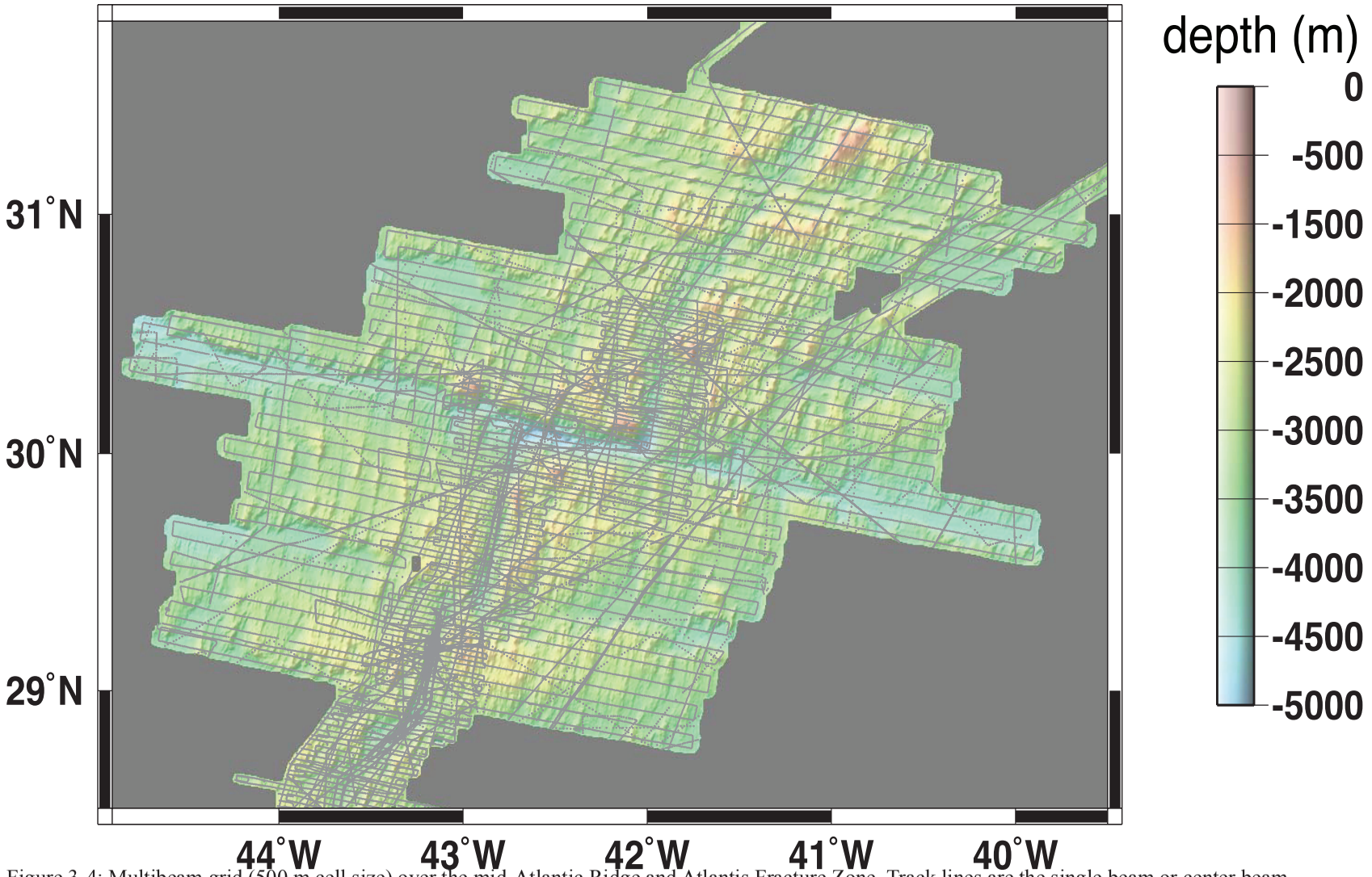

Figure 3-4: Multibeam grid (500 m cell size) over the mid-Atlantic Ridge and Atlantis Fracture Zone. Track lines are the single beam or center beam coverage used to relate 2-D gradients to 1-D slopes.

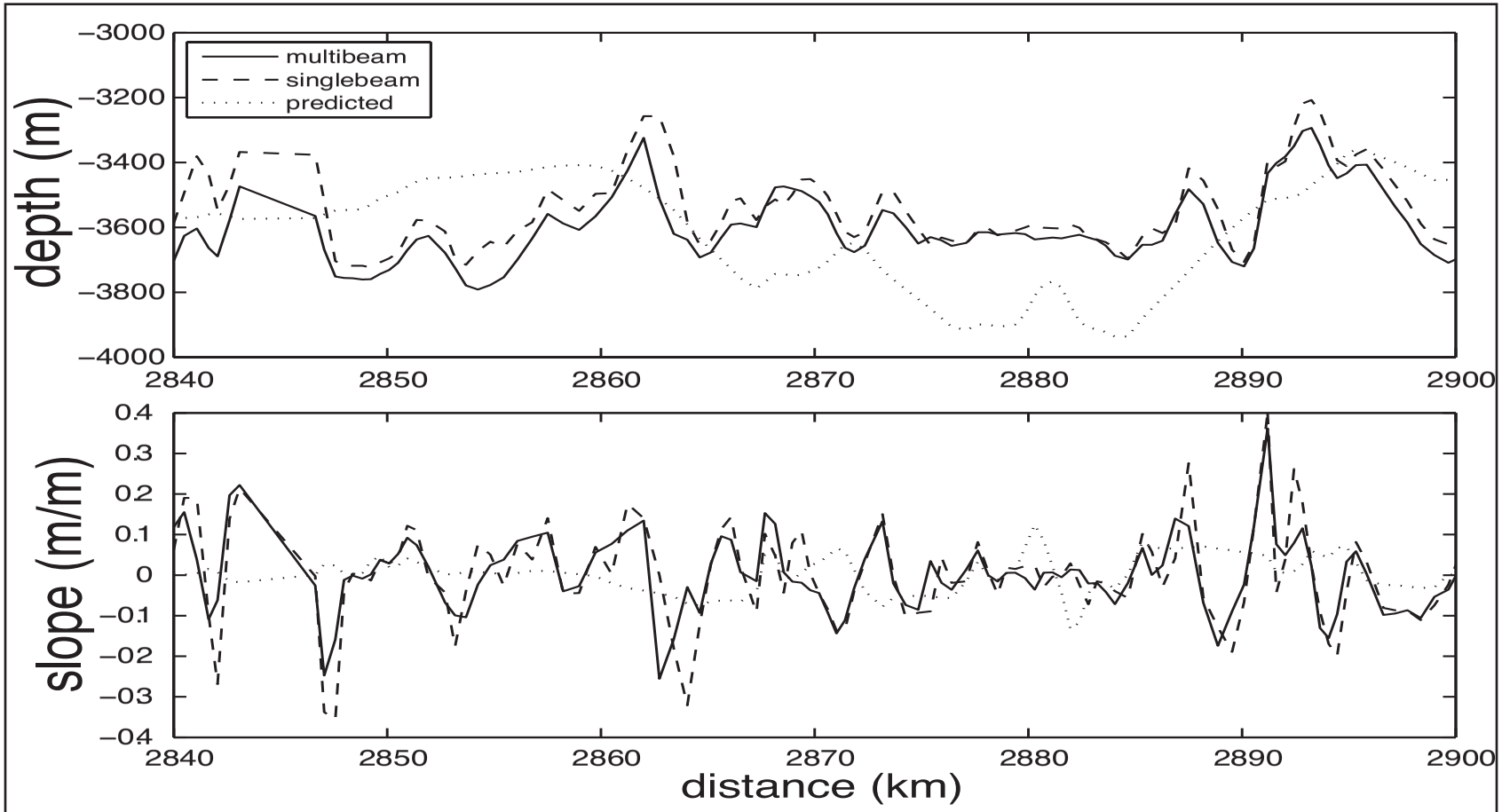

Figure 3-5: Seafloor depth (top) and along-track slope (bottom) along the trackline of a typical cruise near the Mid-Atlantic Ridge (MAR). Multibeam data were sampled from a grid having 500 m cell spacing and represent the "true" depth and slope. Single beam data were filtered and processed along track to best match the multibeam profile. This version of satellite bathymetry was not forced to agree with available soundings so is representative of the accuracy in areas having no shipboard coverage. The rms differences are: single beam depth 48.4 m; satellite bathymetry 190.8 m; single beam slope .066 m/m; multibeam slope .089 m/m.

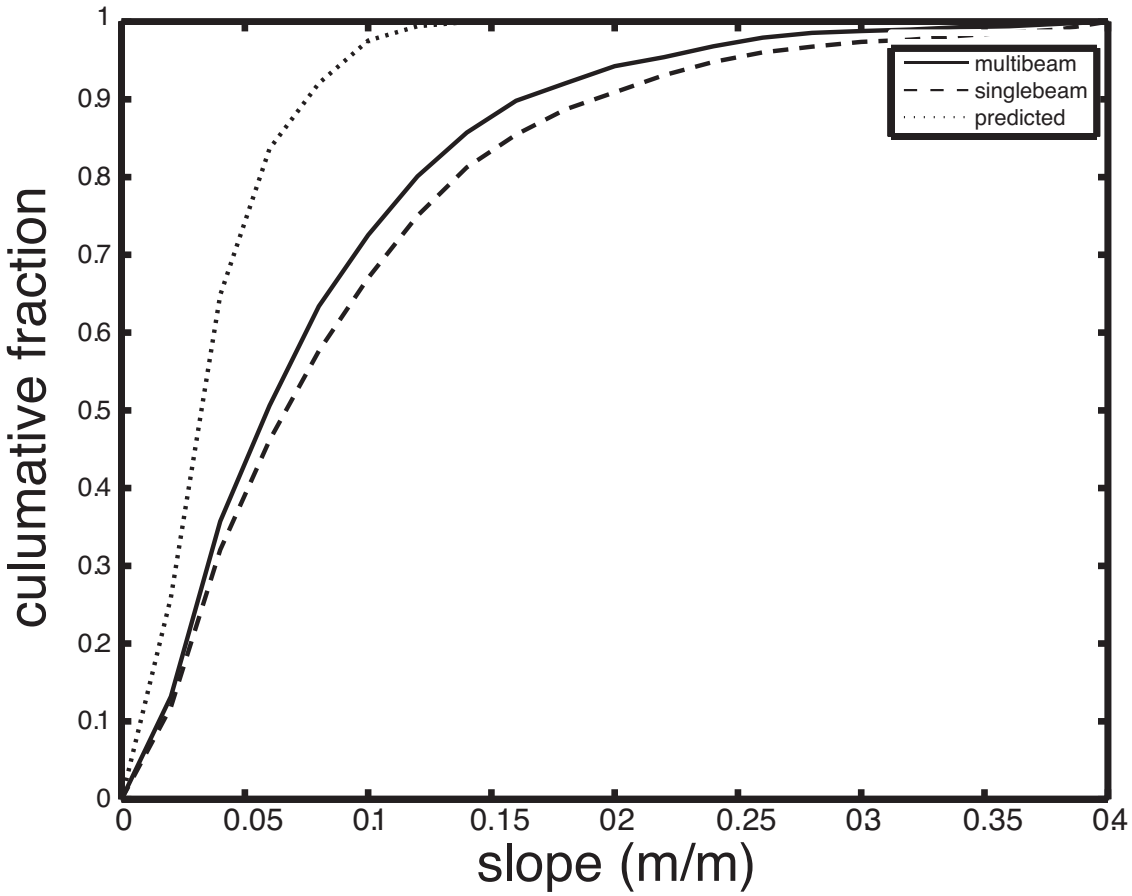

Figure 3-6: Cumulative histograms of the absolute value of the seafloor slope along the trackline from the three measurement systems. 30% of the multibeam and single beam slopes exceed 0.1 m/m, while only 2% of satellite bathymetry slopes exceeds 0.1 m/m.

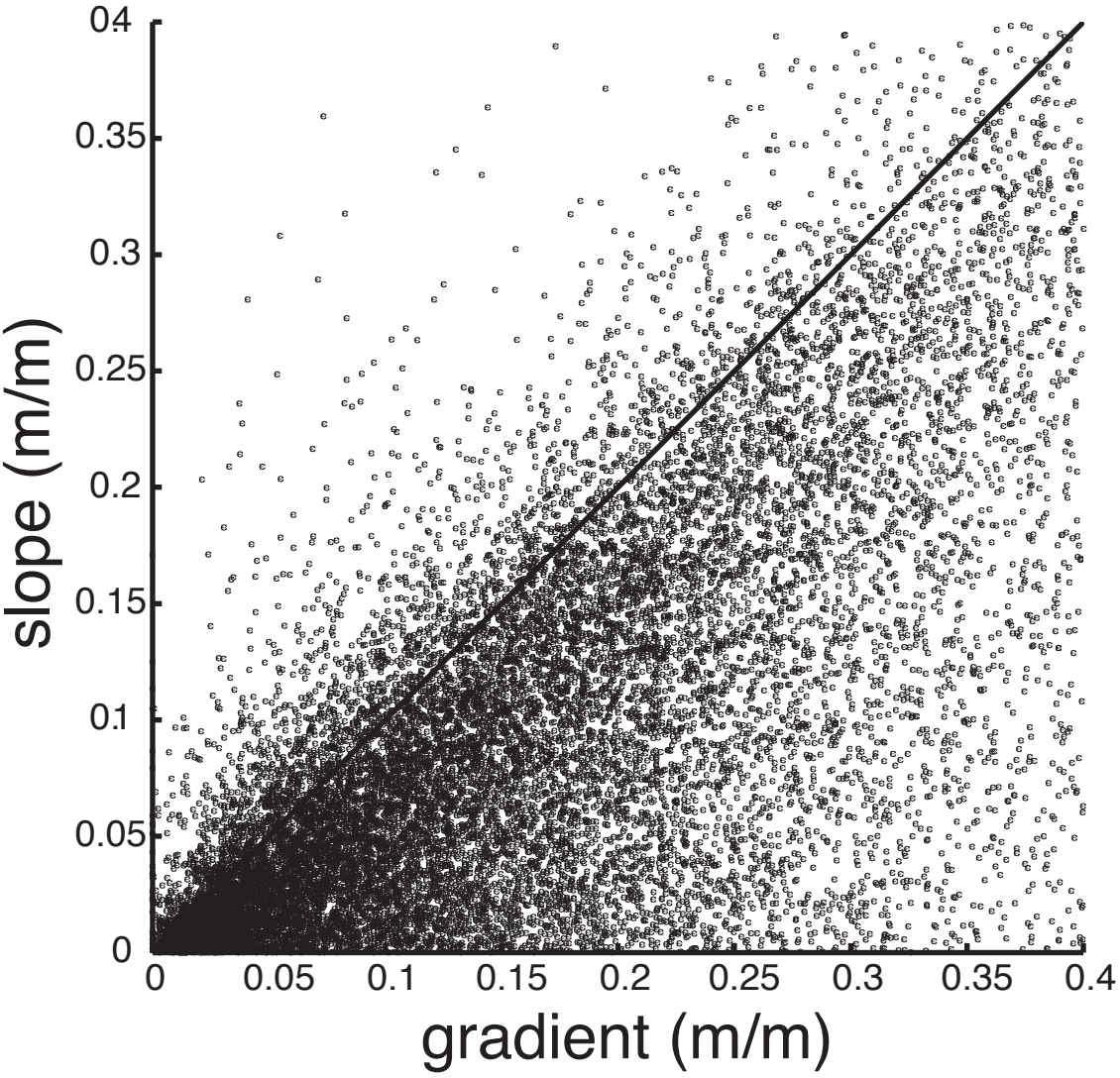

Figure 3-7: Magnitude of along-track slope of the seafloor from single beam data (Figure 1, bottom) versus magnitude of gradient vector at the same locations from a 500-m multibeam grid. Theoretically the 1-D slope should be less than or equal to the 2-D gradient.

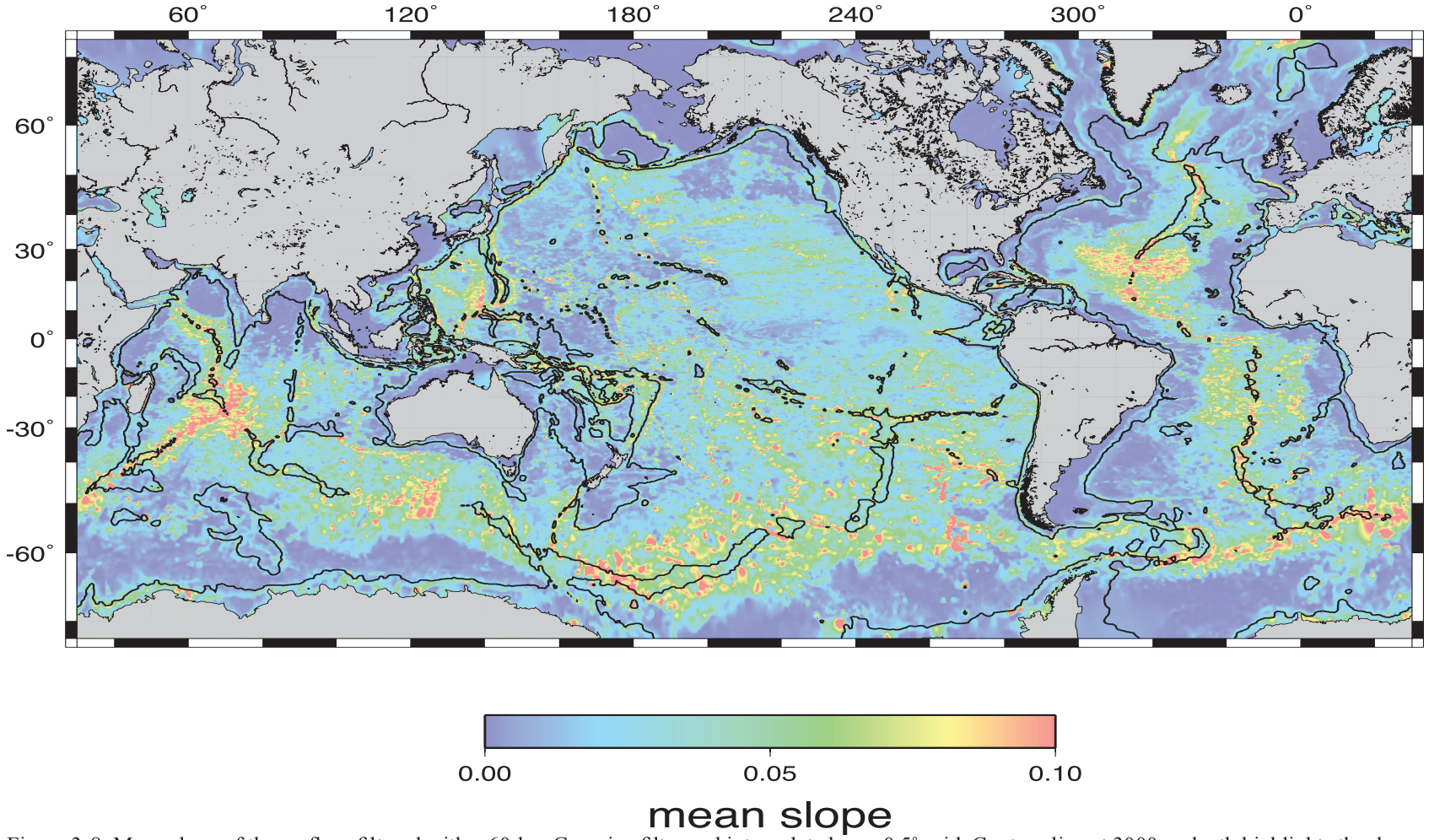

Figure 3-8: Mean slope of the seafloor filtered with a 60-km Gaussian filter and interpolated on a 0.5˚ grid. Contour line at 3000 m depth highlights the deep ocean basins and shows the ridges are not as steep. Mean slope commonly exceeds 0.05 m/m on the flanks of the seafloor spreading ridges, especially the ridges spreading at a rate of < 70 mm/yr.

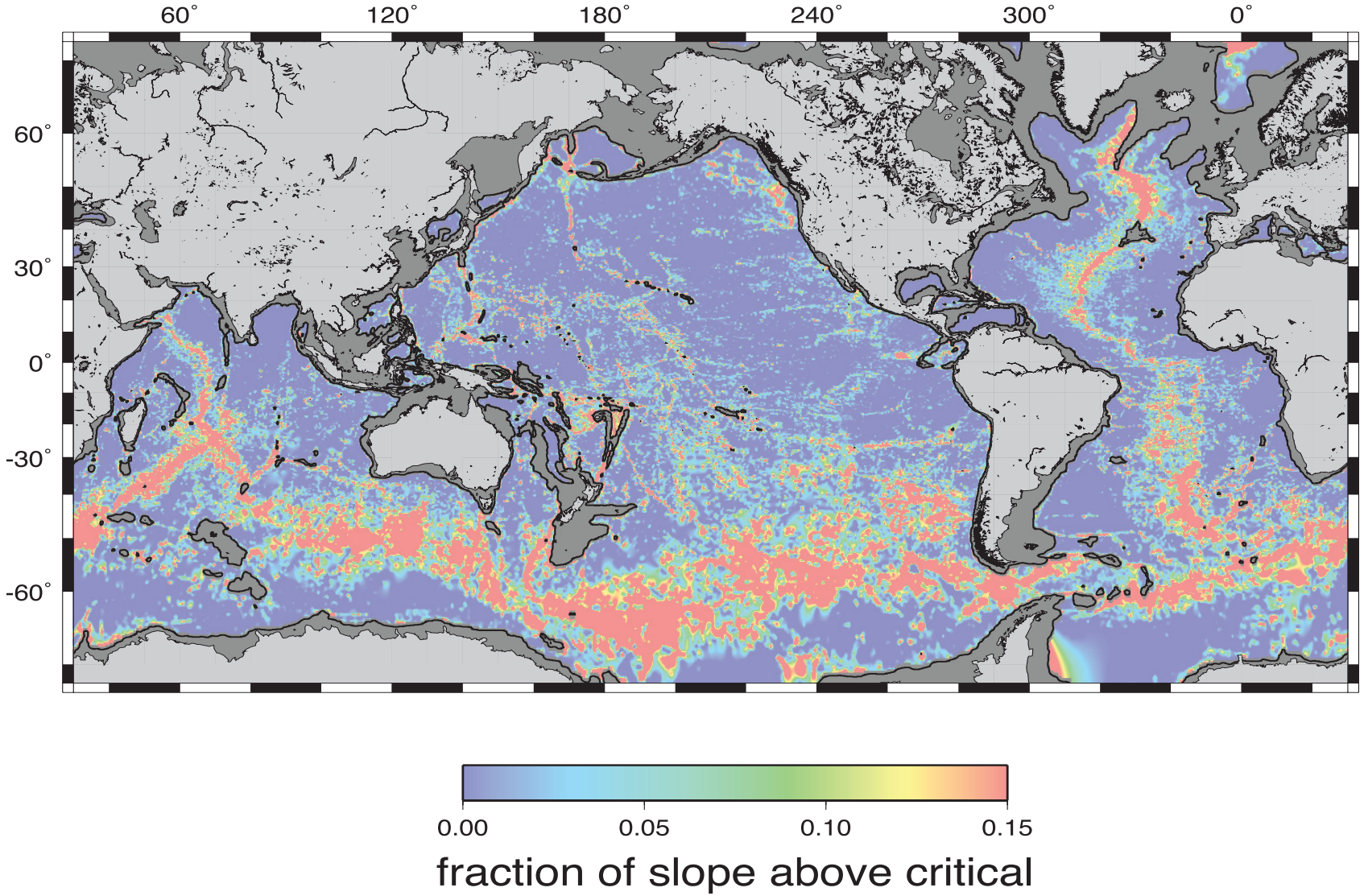

Figure 3-9: Fraction of seafloor having slope exceeding critical slope for depth > 2000 m. Fraction fromsingle beam soundings.

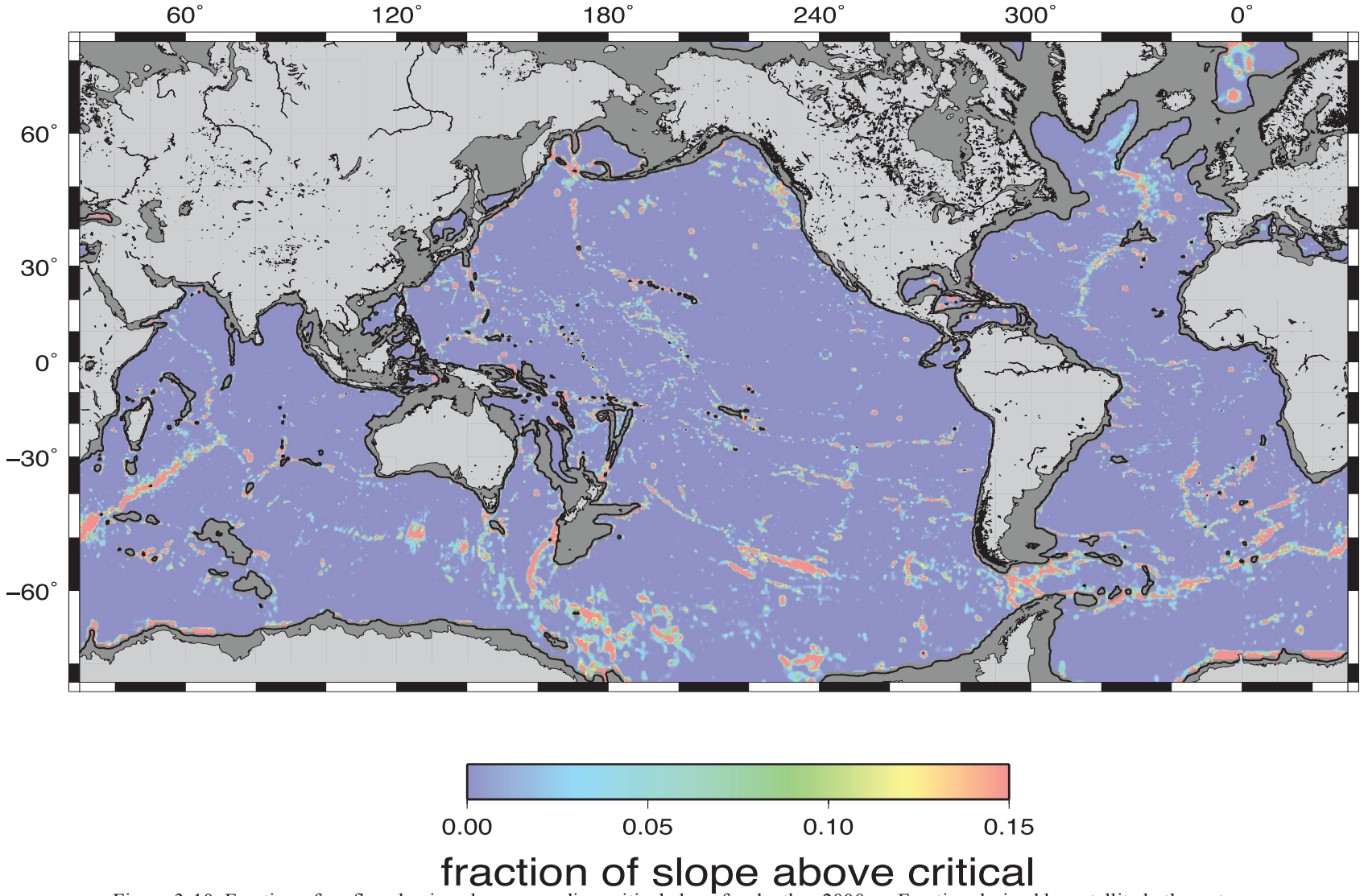

Figure 3-10: Fraction of seafloor having slope exceeding critical slope for depth > 2000 m. Fraction derived by satellite bathymetry

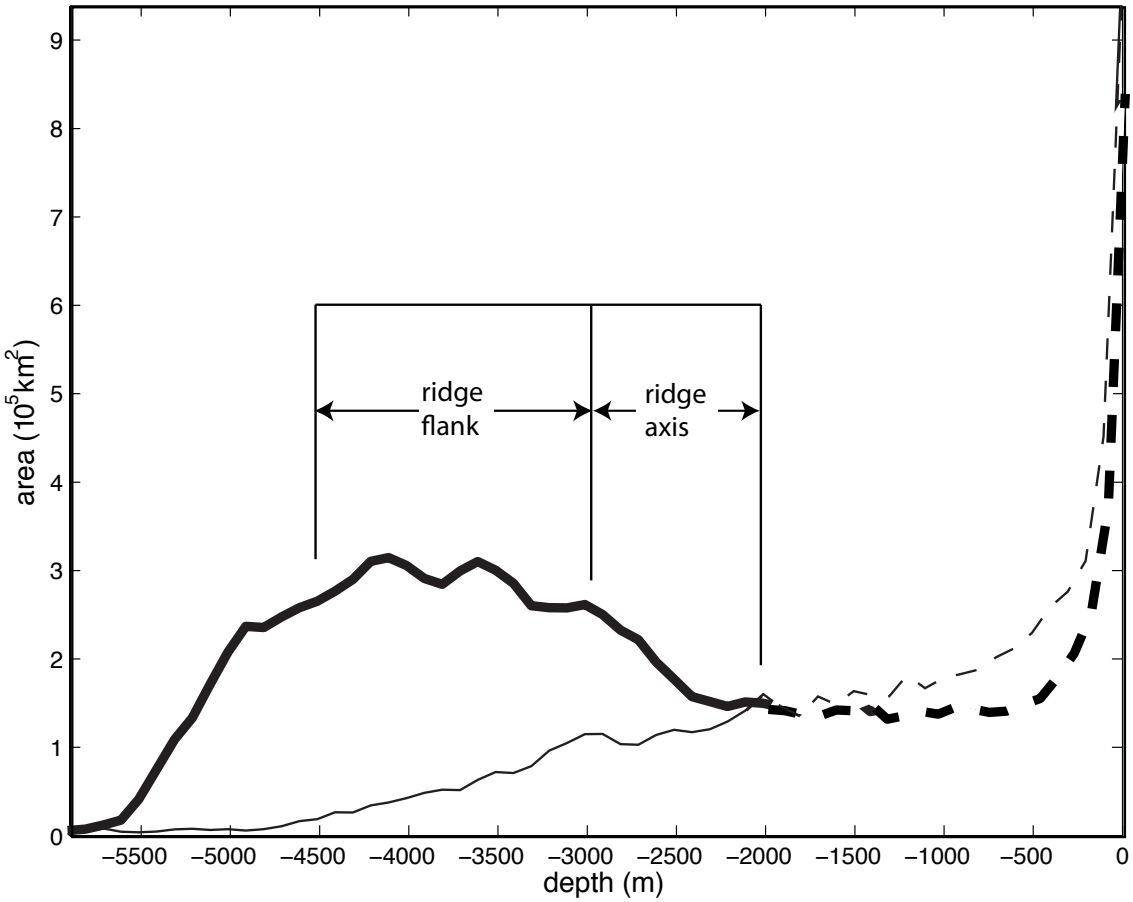

Figure 3-11: Area of seafloor with above critical slope as a function of depth. Thick curve is from single beam data while the thin curve is from satellite bathymetry. Seafloor slopes from satellite bathymetry clearly underestimate supercritical area with depth <2000 m. The critical slope calculation is unreliable for shallow depths < 2000 m.

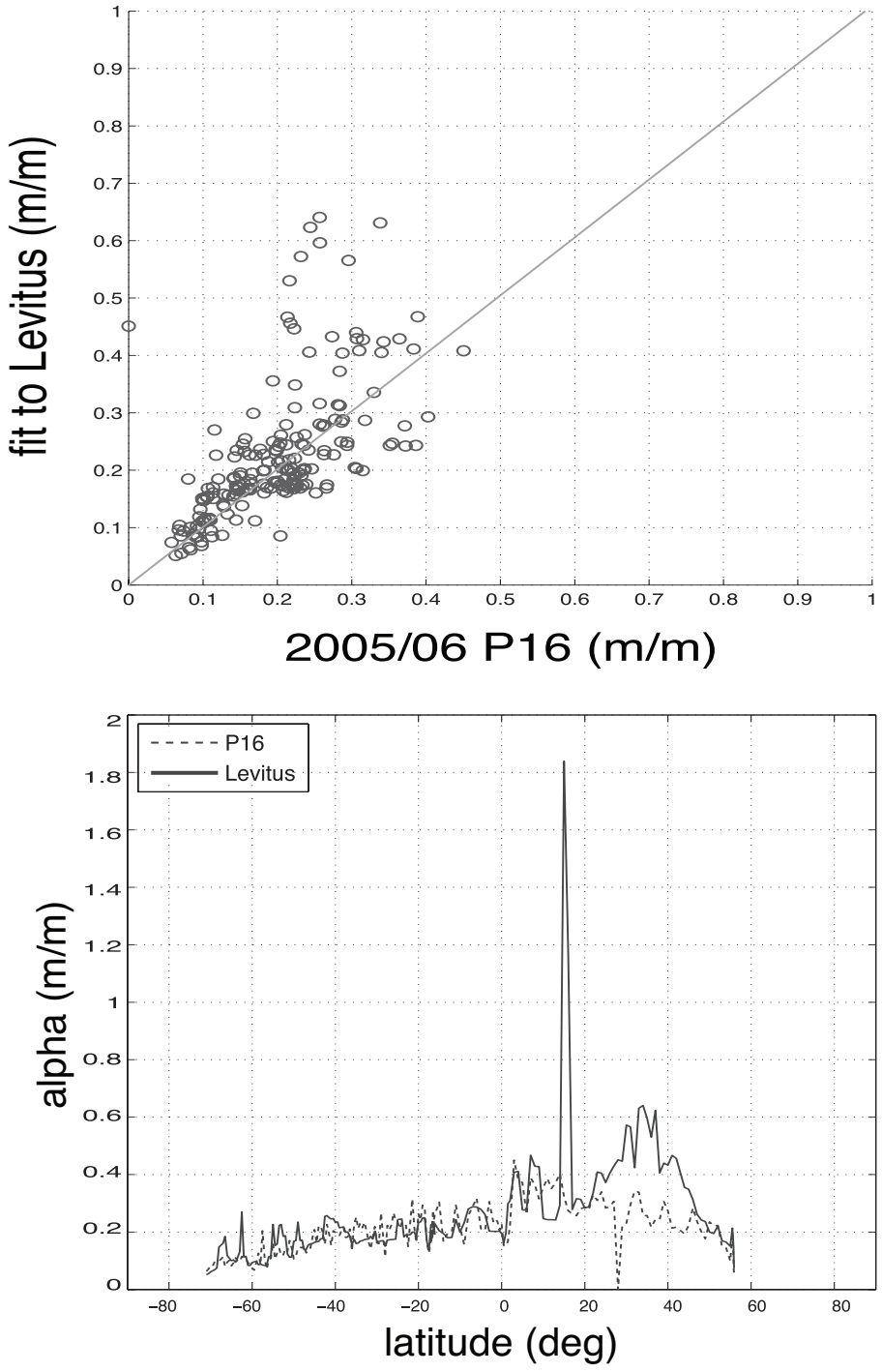

Figure 3-12: Scatter plot of critical slope calculated from WOA and P16 cruise data. (b) Meridional plot of critical slope calculated from WOA and P16 cruise data.

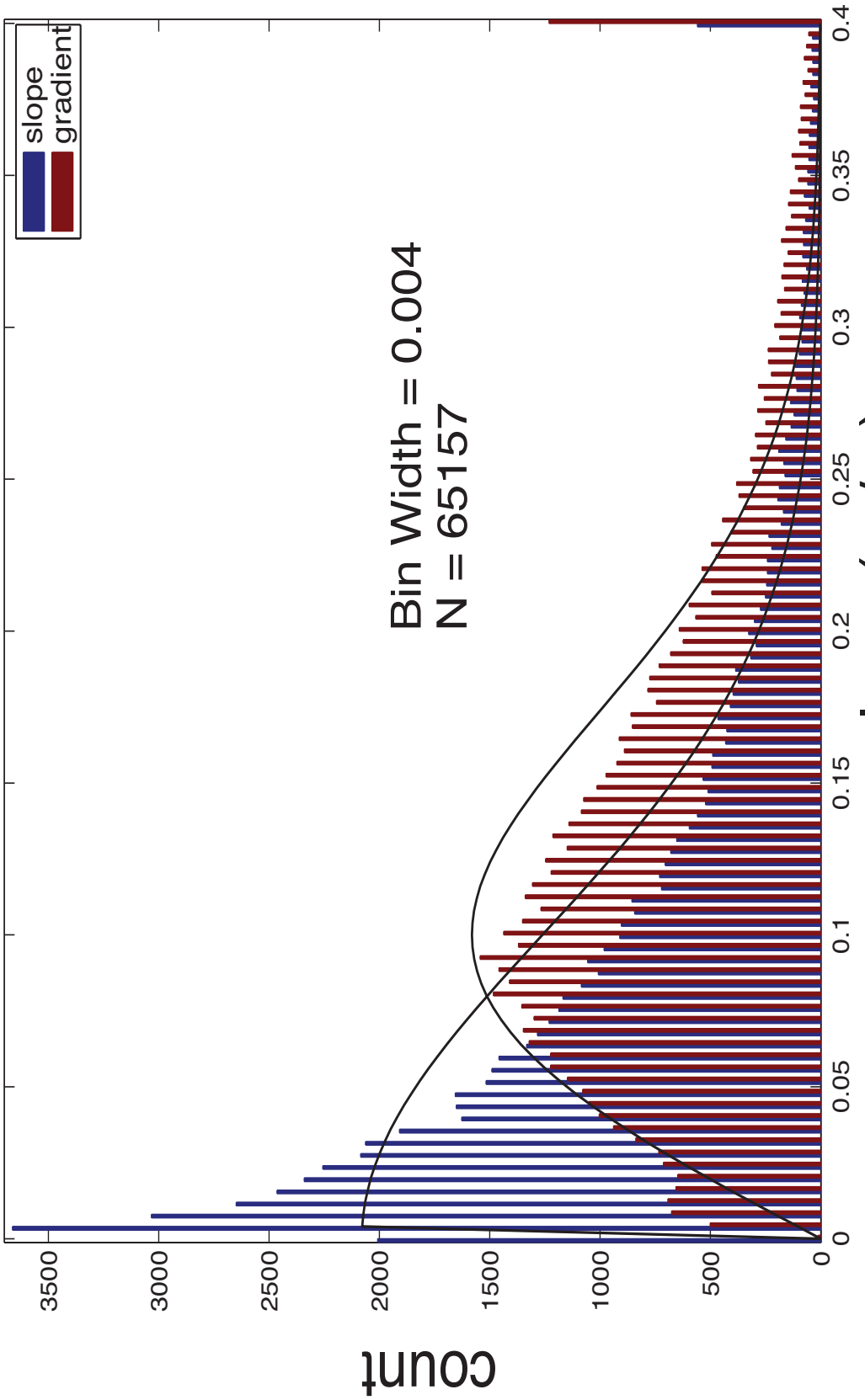

Figure 3-13: Histograms of the magnitude of the slope (blue) and gradient (red) for the data shown in Figure 3-12

4

Conclusion

The results of the previous chapter show there is a large amount of critical topography in the deep ocean that could dissipate the barotropic tides, but rough topography can only dissipate tides if the velocity over it is large. In the absence of a power spectrum, a few qualitative calculations can still be done. As shown in [*Llewellyn Smith and Young*, 2002] tidal dissipation depends on a many factors but the heart of the calculation is

$$\frac{dE}{dt} \sim \nabla h \cdot \overrightarrow{vel} \tag{4-1}$$

However, the orientation of the abyssal hills relative to the deep ocean currents is unknown. To proceed, I ignore the orientation and seek a qualitative description of the dissipation.

Although there are many confounding factors, my thesis is that the tidal dissipation should be large where there is a rapidly moving tide flowing over steep topography. An appropriate time scale would be set by the quality factor or "Q" of the barotropic tide, typically assumed to be about 10. To dissipate its integrated kinetic energy in approximately 10 semidiurnal periods or 10^5 seconds, an area with 1000 joules/m^2 of integrated kinetic energy should dissipate about 10 mW/m^2. Figures 1 and 2 of

[*Egbert and Ray*, 2003] agree with this naïve analysis and encourage further speculation. The integrated kinetic energy (per square meter of surface area) of water with depth H moving in a barotropic tide ignoring upwelling is simplified to be

$$K = \frac{1}{2}\rho H \left\langle vel^2 \right\rangle \tag{4-2}$$

Because the velocity of the tide and the depth of the water are interrelated, the complete equation is important. The bathymetry is known from the results of Chapter 2, the density of seawater is a given, and using the TPXO 6.2 tide model [*Egbert and Erofeeva*, 2004] the time averaged *squared* tidal velocity can be estimated from the tidal ellipse parameters as half the sum of the squares of the semi major and minor axes.

The vertically integrated kinetic energy calculated on a quarter degree grid for the M_2 tide was calculated (Figure 4-1) and verified against figure 2 of [*Egbert and Ray*, 2003]. Multiplying the vertically integrated kinetic energy and the fraction of the sea floor above the M_2 critical slope presented in [*Becker and Sandwell*, 2008] should indicate locations where the water column has a substantial amount of kinetic energy and the seafloor is rough enough to effectively dissipate that barotropic energy (Figure 4-2). The result is certainly ad-hoc, but the result depends only on a well-established tide model and the fraction of sea floor above critical slope presented in chapter 3 and should illustrate if rough topography is a key factor in tidal dissipation. The experimental measurements of dissipation presented in the M_2 tide portion of figure 1 of [*Egbert and Ray*, 2003] do compare well to Figure 4-2.

To begin the qualitative comparisons of Figure 4-2 with [*Egbert and Ray*, 2003] consider the Sea of Okhotsk between the Kamchatka Peninsula and mainland Siberia. The red areas in the northernmost and western portions of the Sea of Okhotsk indicating tidal dissipation in [*Egbert and Ray*, 2003] are seen in Figure 4-2.

The blue area of "negative energy dissipation" seen in [*Egbert and Ray*, 2003] is absent in Figure 4-2. This is encouraging, as negative dissipation is a most likely an

artifact of the difficult calculation presented in [*Egbert and Ray*, 2003]. The lack of "negative dissipation" is on one hand to be expected from the naïve product of kinetic energy and a fraction between zero and one. On the other hand, the absence of "negative dissipation" areas in Figure 4-2 suggests that a naïve calculation is correctly capturing the essence of the tidal dissipation process, and the roughness calculation presented in [*Becker and Sandwell*, 2008] is significant. The agreement to [*Egbert and Ray*, 2003] is imperfect and as some other areas of negative dissipation in [*Egbert and Ray*, 2003] do show up as areas of positive dissipation in Figure 4-2, but generally, the "blue" areas are absent in Figure 4-2.

To the east of Kamchatka, the Aleutian Islands show significant dissipation in both figures. The continental shelf in the Bering Sea is visible in Figure 4-2, and perhaps [*Egbert and Ray*, 2003]. Comparing the area between the Azores and the Canary Islands suggests that [*Egbert and Ray*, 2003] is either not resolving the location of dissipation or the dissipated energy is widely dispersed. Figure 4-2 indicates that the Azores, the seamounts south of the Azores and the Canary Islands are strong point dissipaters in an otherwise quiet area. [*Egbert and Ray*, 2003] shows a diffuse area of increased dissipation. This is consistent with other areas such as Tuamotu Archipelago where point sources in Figure 4-2 are seen as broad diffuse areas in [*Egbert and Ray*, 2003].

Hawaii is prominent in Figure 4-2, but not in [*Becker and Sandwell*, 2008]. This is an area where a relatively small and isolated patch of critical slope is located in an area of strong currents. In comparison, the larger areas of critical slope in the Southern Ocean are not visible in Figure 4-2, or [*Egbert and Ray*, 2003], because they do not experience strong tides. The critical slope areas of the Southern Ocean could still contribute to mixing by interacting with the Antarctic Circumpolar Current rather than the barotropic tide.

Many other areas of agreement between Figure 4-2 and [*Egbert and Ray*, 2003]

are visible such as the Caribbean Trench, the Brazil Basin, the ridge extending south from Japan, the Indonesian Archipelago, both ends of Madagascar, New Zealand, Hudson's Bay and Cape Horn. This general agreement strongly suggests that M_2 dissipation is dominated by super critical seafloor in areas of strong tidal currents. Further research is needed to quantify these results and explain the few discrepancies between Figure 4-2 and [*Egbert and Ray*, 2003] such as the Northern MAR and the continental shelf of Argentina. A relatively simple test that should be done is to calculate the diurnal critical slope fraction and compare that to [*Egbert and Ray*, 2003].

Comparing the qualitative results of [*Becker and Sandwell*, 2008] to tidal dissipation measurements such as [*Egbert and Ray*, 2000; 2001; 2003; *Rudnick et al.*, 2003] is simple, but a quantitative calculation requires additional research. A complete calculation of the barotropic tide dissipation involves the two dimensional power spectrum of the topography, and that spectrum is not available. A time consuming preliminary investigation into estimating the 2-d power spectrum using single beam data appears promising. The initial indication is that the knee in the widely cited Goff spectrum [*Goff and Jordan*, 1988] may be an artifact reflecting the length of the data window. The knee of the curve is the low frequency roll off of a red spectrum measured at wavelengths approaching the length of the data window. This is easily seen by calculating the spectrums of a very long ship track, and the spectrum of both halves of that ship track, and so on. If the corner frequency were a physical process the knee frequency visible at long wavelengths of the larger window would be absent in smaller windows that do not include that knee frequency. The knee is always present and at about half the window length used, showing it is simply an artifact when measuring the spectrum of the sea floor. However, the results in [*Goff and Jordan*, 1988] apply only to the abyssal hill fabric and not the entire sea floor. This distinction is important.

The 1-d spectrum calculation holds promise for doing an accurate barotropic

tidal dissipation calculation. The [*Nycander*, 2005] results indicate that the spectrum at wavelengths as small as one km have an inordinate effect on the dissipation. The preliminary power spectrum results indicate it may be able to estimate the power spectrum at such high frequencies, however the usual complexities arising from real data processing remain to be addressed before a calculation extending the results of [*Nycander*, 2005] can be done.

In parting I'd like to once again thank my committee and the entire SIO community. It has been a fabulous ride.

4.1 REFERENCES

Becker, J. J., and D. T. Sandwell (2008), Global Estimates of Seafloor Slope from Single-Beam Ship Soundings, *J. Geophys. Res.*

Egbert, G. D., and R. D. Ray (2000), Significant dissipation of tidal energy in the deep ocean inferred from satellite altimeter data, *Nature*, *405*(6788), 775-778.

Egbert, G. D., and R. D. Ray (2001), Estimates of M-2 tidal energy dissipation from TOPEX/Poseidon altimeter data, *Journal of Geophysical Research-Oceans*, *106*(C10), 22475-22502.

Egbert, G. D., and R. D. Ray (2003), Semi-diurnal and diurnal tidal dissipation from TOPEX/Poseidon altimetry, *Geophysical Research Letters*, *30*(17), -.

Egbert, G. D., and S. Y. Erofeeva (28 Nov. 2005). TPXO6.2: Global Inverse Tide Model Version 1.2. http://www.esr.org/polar_tide_models/Model_TPXO62.html (6 Mar. 2008).

Goff, J. A., and T. H. Jordan (1988), Stochastic Modeling of Seafloor Morphology - Inversion of Sea Beam Data for 2nd-Order Statistics, *Journal of Geophysical Research-Solid Earth and Planets*, *93*(B11), 13589-13608.

Llewellyn Smith, S. G., and W. R. Young (2002), Conversion of the barotropic tide, *Journal of Physical Oceanography*, *32*(5), 1554-1566.

Nycander, J. (2005), Generation of internal waves in the deep ocean by tides., *Journal of geophysical research*, *110*(c10), C10028-.

Rudnick, D. L., et al. (2003), From tides to mixing along the Hawaiian ridge, *Science*, *301*(5631), 355-357.

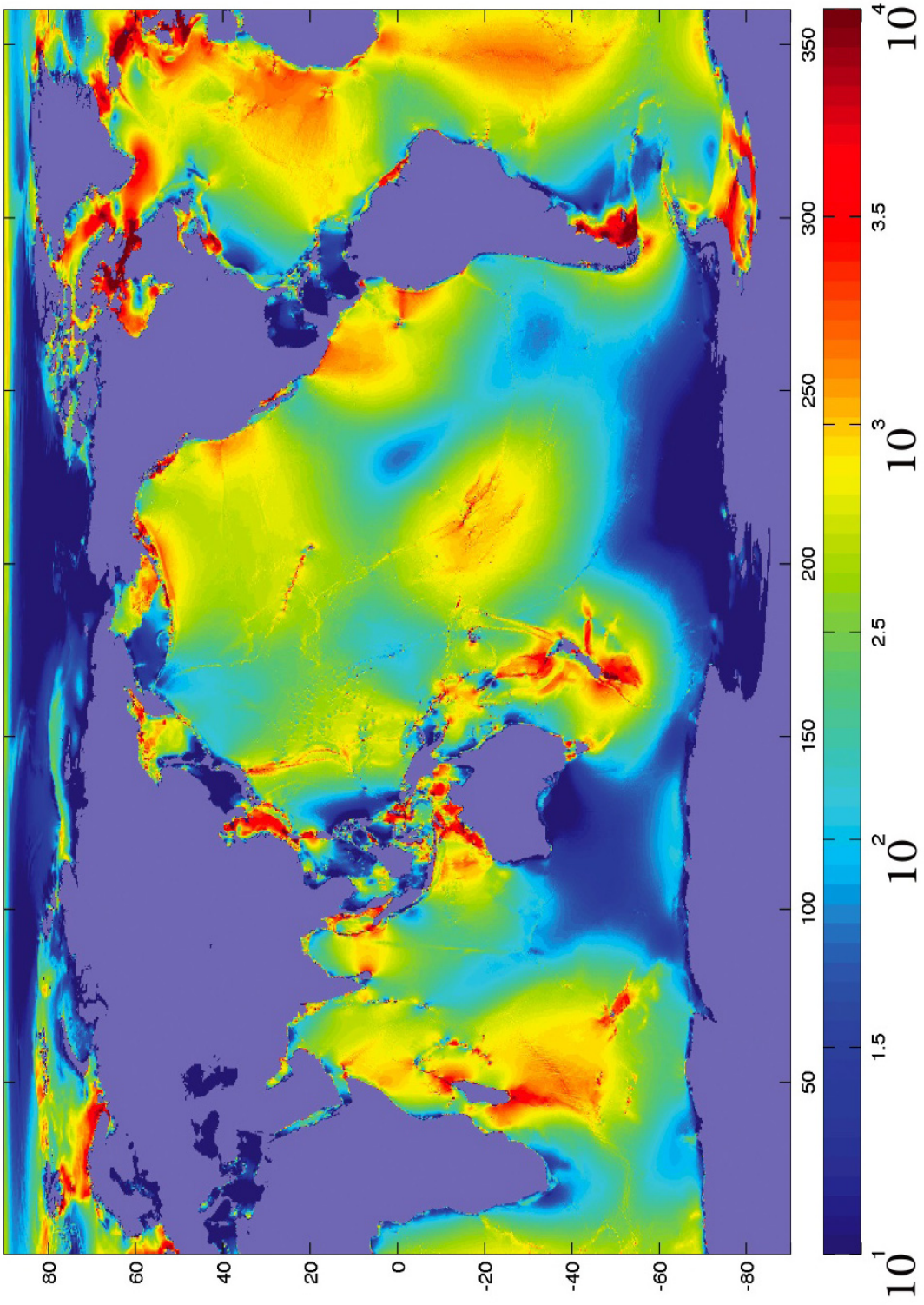

Figure 4-1: Vertically integrated kinetic energy of the M_2 tide (J/m^2)

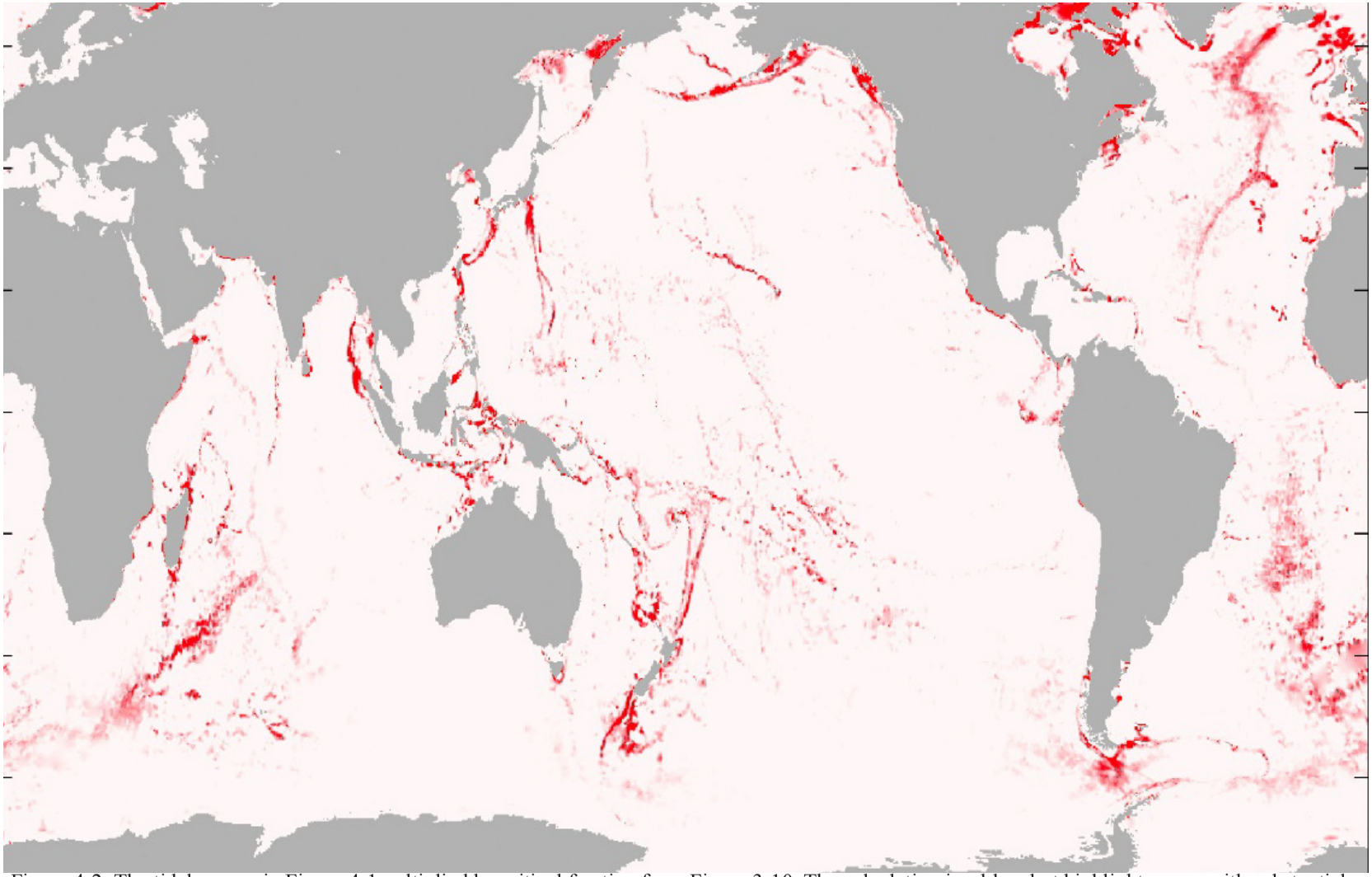

Figure 4-2: The tidal energy in Figure 4-1multiplied by critical fraction from Figure 3-10. The calculation is ad-hoc but highlights areas with substantial kinetic energy in the M2 tide and a rough sea floor. Such areas would be expected to dissipate the barotropic tide. The units are arbitrary, but linear.